



**HAL**  
open science

## **Plasmodium vivax binds host CD98hc (SLC3A2) to enter immature red blood cells**

Benoît Malleret, Abbas El Sahili, Matthew Zirui Tay, Guillaume Carissimo, Alice Soh Meoy Ong, Wisna Novera, Jianqing Lin, Rossarin Suwanarusk, Varakorn Kosaisavee, Trang Chu, et al.

► **To cite this version:**

Benoît Malleret, Abbas El Sahili, Matthew Zirui Tay, Guillaume Carissimo, Alice Soh Meoy Ong, et al.. Plasmodium vivax binds host CD98hc (SLC3A2) to enter immature red blood cells. Nature Microbiology, 2021, 6 (8), pp.991-999. 10.1038/s41564-021-00939-3 . hal-03448619

**HAL Id: hal-03448619**

**<https://hal.science/hal-03448619>**

Submitted on 25 Nov 2021

**HAL** is a multi-disciplinary open access archive for the deposit and dissemination of scientific research documents, whether they are published or not. The documents may come from teaching and research institutions in France or abroad, or from public or private research centers.

L'archive ouverte pluridisciplinaire **HAL**, est destinée au dépôt et à la diffusion de documents scientifiques de niveau recherche, publiés ou non, émanant des établissements d'enseignement et de recherche français ou étrangers, des laboratoires publics ou privés.



# *Plasmodium vivax* binds host CD98hc (SLC3A2) to enter immature red blood cells

Benoît Malleret<sup>1,2,3</sup>✉, Abbas El Sahili<sup>4,5,24</sup>, Matthew Zirui Tay<sup>1,6,24</sup>, Guillaume Carissimo<sup>1,6,24</sup>, Alice Soh Meoy Ong<sup>1,6</sup>, Wisna Novera<sup>7</sup>, Jianqing Lin<sup>4,6</sup>, Rossarin Suwanarusk<sup>1,8</sup>, Varakorn Kosaisavee<sup>2,8,9</sup>, Trang T. T. Chu<sup>10</sup>, Ameya Sinha<sup>10</sup>, Shanshan Wu Howland<sup>1</sup>, Yiping Fan<sup>11,12</sup>, Jakub Gruszczyk<sup>13</sup>, Wai-Hong Tham<sup>13,14</sup>, Yves Colin<sup>15,16</sup>, Sebastian Maurer-Stroh<sup>16,17,18</sup>, Georges Snounou<sup>19</sup>, Lisa F. P. Ng<sup>1,6</sup>, Jerry Kok Yen Chan<sup>11,12,20</sup>, Ann-Marie Chacko<sup>1</sup>, Julien Lescar<sup>1,4,5</sup>, Rajesh Chandramohanadas<sup>2,10</sup>, François Nosten<sup>1,21,22</sup>, Bruce Russell<sup>1,2,8,24</sup> and Laurent Rénia<sup>1,6,23,24</sup>✉

**More than one-third of the population of the world is exposed to *Plasmodium vivax* malaria, mainly in Asia<sup>1</sup>. *P. vivax* preferentially invades reticulocytes (immature red blood cells)<sup>2-4</sup>. Previous work has identified 11 parasite proteins involved in reticulocyte invasion, including erythrocyte binding protein 2 (ref. <sup>5</sup>) and the reticulocyte-binding proteins (PvRBPs)<sup>6-10</sup>. PvRBP2b binds to the transferrin receptor CD71 (ref. <sup>11</sup>), which is selectively expressed on immature reticulocytes<sup>12</sup>. Here, we identified CD98 heavy chain (CD98), a heteromeric amino acid transporter from the SLC3 family (also known as SLCA2), as a reticulocyte-specific receptor for the PvRBP2a parasite ligand using mass spectrometry, flow cytometry, biochemical and parasite invasion assays. We characterized the expression level of CD98 at the surface of immature reticulocytes (CD71<sup>+</sup>) and identified an interaction between CD98 and PvRBP2a expressed at the merozoite surface. Our results identify CD98 as an additional host membrane protein, besides CD71, that is directly associated with *P. vivax* reticulocyte tropism. These findings highlight the potential of using PvRBP2a as a vaccine target against *P. vivax* malaria.**

The development of malaria infection depends on the efficiency with which the invasive forms, merozoites, attach to and invade erythrocytes. Red blood cell (RBC) selection is not random, as the tropism towards erythrocytes of different ages varies with

*Plasmodium* species and restrict zoonotic infections<sup>13,14</sup>. Furthermore, merozoite invasion occurs within minutes, and while free in the blood stream, these forms are particularly vulnerable to immune attack<sup>15</sup>. To take advantage of this brief window of opportunity, targeting the molecules implicated in RBC selection and invasion is attractive for vaccine development. This has prompted sustained efforts to unravel the complex sequence of events leading to erythrocyte invasion and to identify the parasite and host proteins that mediate them.

Knowledge of erythrocyte invasion has been mainly accrued for *Plasmodium falciparum*, a parasite that can invade all erythrocyte subsets, through detailed and elegant investigations made possible by the ability to culture this species in vitro and to generate genetic variants. This has led to the discovery of multiple combinations of parasite ligands and host receptors that mediate distinct invasion pathways, with the most recent PfRh5-basigin combination providing a particularly promising target for vaccine development<sup>16,17</sup>. In contrast, invasion by *P. vivax*, a species long known to have a strict predilection towards reticulocytes<sup>2-4</sup>, cannot be adequately continuously maintained in vitro and has consequently been far less studied. We have previously shown that the *P. vivax* merozoite preferentially targets reticulocytes expressing the immature reticulocyte marker CD71 (ref. <sup>4</sup>). Gruszczyk et al.<sup>11</sup> then identified CD71 (transferrin receptor 1)

<sup>1</sup>Singapore Immunology Network (SigN), Agency for Science Technology and Research (A\*STAR), Biopolis, Singapore. <sup>2</sup>Department of Microbiology and Immunology, Yong Loo Lin School of Medicine, National University of Singapore, Singapore, Singapore. <sup>3</sup>Immunology Translational Research Programme, Yong Loo Lin School of Medicine, Immunology Programme, Life Sciences Institute, National University of Singapore, Singapore, Singapore. <sup>4</sup>School of Biological Sciences, Nanyang Technological University, Singapore, Singapore. <sup>5</sup>NTU Institute for Structural Biology, Nanyang Technological University, Singapore, Singapore. <sup>6</sup>A\*STAR ID Labs, Agency for Science Technology and Research (A\*STAR), Biopolis, Singapore. <sup>7</sup>Laboratory for Translational and Molecular Imaging, Cancer and Stem Cell Biology Programme, Duke-NUS Medical School, Singapore, Singapore. <sup>8</sup>Department of Microbiology and Immunology, University of Otago, Dunedin, New Zealand. <sup>9</sup>Department of Parasitology and Entomology, Faculty of Public Health, Mahidol University, Bangkok, Thailand. <sup>10</sup>Pillar of Engineering Product Development, Singapore University of Technology & Design, Singapore, Singapore. <sup>11</sup>Department of Reproductive Medicine, KK Women's and Children's Hospital, Singapore, Singapore. <sup>12</sup>Experimental Fetal Medicine Group, Department of Obstetrics and Gynecology, Yong Loo Lin School of Medicine, National University of Singapore, Singapore, Singapore. <sup>13</sup>The Walter and Eliza Hall Institute of Medical Research, Parkville, Victoria, Australia. <sup>14</sup>Department of Medical Biology, The University of Melbourne, Melbourne, Victoria, Australia. <sup>15</sup>Université de Paris, UMR\_S1134, BIGR, INSERM, Paris, France. <sup>16</sup>Institut National de Transfusion Sanguine, Paris, France. <sup>17</sup>Bioinformatics Institute, Agency for Science Technology and Research (A\*STAR), Biopolis, Singapore. <sup>18</sup>Department of Biological Sciences, National University of Singapore, Singapore, Singapore. <sup>19</sup>CEA-Université Paris Sud 11-INSERM U1184, Immunology of Viral Infections and Autoimmune Diseases (IMVA-HB), IDMIT Department, IBFJ, DRF, Fontenay-aux-Roses, France. <sup>20</sup>Academic Clinical Program in Obstetrics and Gynecology, Duke-NUS Medical School, Singapore, Singapore. <sup>21</sup>Shoklo Malaria Research Unit, Mahidol-Oxford Tropical Medicine Research Unit, Faculty of Tropical Medicine, Mahidol University, Mae Sot, Thailand. <sup>22</sup>Centre for Tropical Medicine, Nuffield Department of Medicine, University of Oxford, Oxford, UK. <sup>23</sup>Lee Kong Chian School of Medicine, Nanyang Technological University, Singapore, Singapore. <sup>24</sup>These authors contributed equally: Abbas El Sahili, Matthew Zirui Tay, Guillaume Carissimo, Bruce Russell and Laurent Rénia. ✉e-mail: [Benoit\\_Malleret@immunol.a-star.edu.sg](mailto:Benoit_Malleret@immunol.a-star.edu.sg); [Renia\\_Laurent@immunol.a-star.edu.sg](mailto:Renia_Laurent@immunol.a-star.edu.sg)

64 as a reticulocyte receptor recognized by the merozoite protein  
65 PvRBP2b. However, previous studies of different *P. vivax* strains  
66 from Brazil<sup>18</sup> and Thailand<sup>19</sup> have shown that merozoite invasion is  
67 trypsin-resistant. CD71 is trypsin sensitive (Fig. 1a), which suggests  
68 the possibility of an alternative receptor on reticulocytes for *P. vivax*  
69 merozoites. This hypothesis was recently supported by a study<sup>20</sup>  
70 demonstrating that merozoite invasion could not be prevented by  
71 antibodies against CD71.

72 To find potential targets that are differentially expressed by  
73 this susceptible cell population, we followed a strategy of a dif-  
74 ferential proteomics screen of CD71<sup>+</sup> (susceptible) versus CD71<sup>-</sup>  
75 (non-susceptible) erythrocyte ghost membranes. Candidate  
76 reticulocyte-specific receptors were selected on the basis of the  
77 following two criteria: (1) abundant expression on CD71<sup>+</sup> imma-  
78 ture reticulocytes but not on CD71<sup>-</sup> normocytes and (2) resistance  
79 to trypsin treatment. The proteomics screen identified a number  
80 of proteins with increased expression on CD71<sup>+</sup> reticulocytes<sup>21</sup>  
81 (Fig. 1b), of which a subset was resistant to trypsin treatment  
82 as demonstrated by flow cytometry (Extended Data Fig. 1 and  
83 Supplementary Table 1). Two surface proteins displayed a significant  
84 fold-change reduction in their expression levels between CD71<sup>+</sup> and  
85 CD71<sup>-</sup> erythrocytes, namely CD71 (~6-fold) and CD98 (~4-fold),  
86 while all others showed less than a 2-fold change (Fig. 1b). Of these  
87 two proteins, only CD98 proved resistant to trypsin treatment  
88 (Extended Data Fig. 1). The decrease in CD98 expression during  
89 cord blood erythrocyte maturation from CD71<sup>+</sup> to CD71<sup>-</sup> erythro-  
90 cytes was confirmed by careful immunophenotyping (Fig. 1c). The  
91 population of CD71<sup>+</sup>CD98<sup>+</sup> reticulocytes represents a minor frac-  
92 tion of RBCs and reticulocytes in adult peripheral blood (Extended  
93 Data Fig. 2a). A decrease in CD98 expression during erythrocyte  
94 maturation was also confirmed by immunofluorescence (Fig. 1d)  
95 and western blotting (Fig. 1e) analyses of in vitro-matured CD71<sup>+</sup>  
96 reticulocytes. CD98 (also known as SLC3A2 or 4F2hc) is the heavy  
97 chain component of the large neutral amino acid transporter com-  
98 plex<sup>22,23</sup> that is peripherally expressed on the reticulocyte mem-  
99 brane<sup>24–27</sup> (Fig. 1f).

100 To demonstrate the involvement of CD98 in the invasion of  
101 reticulocytes, we conducted invasion inhibition assays using differ-  
102 ent *P. vivax* clinical isolates<sup>28</sup>. Anti-CD98 antibodies significantly  
103 abrogated the invasion of *P. vivax* merozoites into CD71<sup>+</sup> reticulo-  
104 cytes, with high levels of inhibition (~70%; Fig. 2). Conversely, anti-  
105 bodies directed against three other erythrocyte membrane proteins,  
106 CD240DCE (Rh), CD99 and CD147 (basigin), a known receptor of  
107 *P. falciparum* merozoite invasion<sup>16</sup>, had little to no effect on invasion  
108 efficiency (Fig. 2). All of the *P. vivax* clinical isolates from Thailand  
109 used in this study and previous studies<sup>10,28</sup> were DARC dependent  
110 (>95% inhibition of invasion; Fig. 2). It is interesting to note that in  
111 the patient samples, CD98 could not be detected at the surface of the  
112 *P. vivax*-infected reticulocytes at the ring stage. This suggests that  
113 CD98 expression on the cell surface is lost soon after invasion of  
114 reticulocytes by *P. vivax* (Extended Data Fig. 2b,c), a phenomenon  
115 also seen for CD71 (ref. 4).

To identify the corresponding parasite ligand that binds CD98,  
we generated a small pDisplay surface-expression library of selected  
*P. vivax* genes, such as the RBPs, which are potentially implicated in  
merozoite invasion (Extended Data Fig. 3a–c and Supplementary  
Table 2). The *P. vivax* antigen library, cloned in the pDisplay vec-  
tor, consisted of 28 different constructs encoding for 7 different *P.*  
*vivax* proteins that were successfully transfected into HEK293 cells  
for cell surface expression. Binding assays using these cells with  
CD71<sup>+</sup> immature versus CD71<sup>-</sup> mature erythrocytes identified  
fragments encoded by two genes, *PvRBP2a* (Fig. 3) and *PvRBP2b*  
(Supplementary Table 2), that mediated strong binding to imma-  
ture reticulocytes. To determine which of these were the cognate  
target for CD98, anti-CD98 antibodies were used to block their  
binding. *PvRBP2a* binding was blocked by anti-CD98 antibod-  
ies (Fig. 3b,c). By contrast, the same anti-CD98 antibodies could  
not block *PvRBP2b* binding (Extended Data Fig. 3e), which was  
expected since *PvRBP2b* has been shown to bind to CD71 (ref. 11).  
*PvRBP2a* was also capable of binding to normocytes, but this inter-  
action was not blocked by anti-CD98 antibodies (Extended Data  
Fig. 3f). These observations also indicate that the *PvRBP2a* protein  
can bind additional proteins on the surface of normocytes.

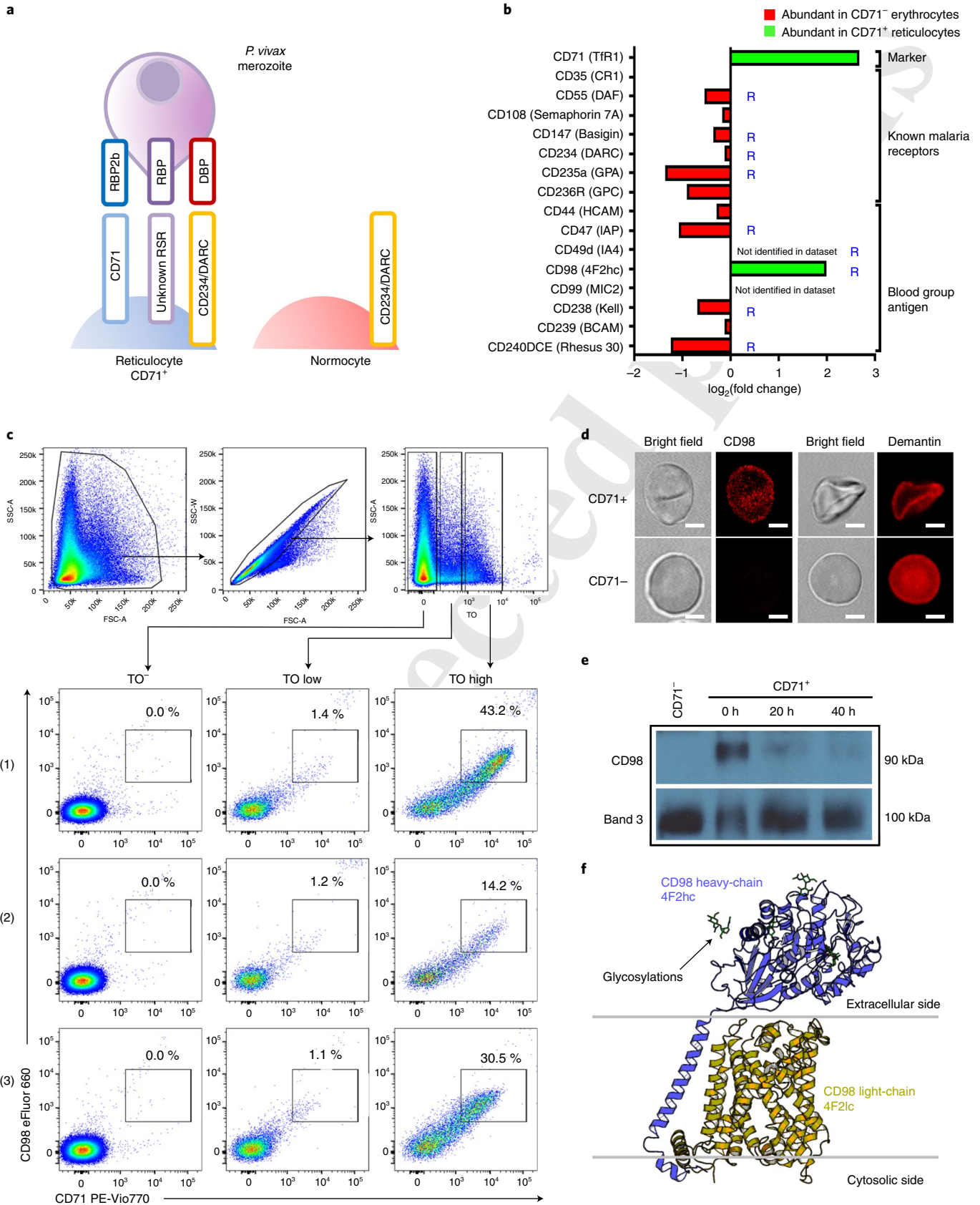
The highest level of binding with reticulocytes, more than two-  
fold than that measured for the other constructs, was observed  
with HEK293 cells displaying *PvRBP2a*<sub>23–767</sub>. HEK293 cells trans-  
fected with constructs corresponding to other regions of *PvRBP2a*  
showed weaker but still significant binding (Fig. 3a, Extended Data  
Fig. 3b and Supplementary Table 2). Binding of cells transfected  
with the *PvRBP2a*<sub>23–767</sub> construct to reticulocytes was abolished by  
the presence of two different clones of anti-*PvRBP2a* monoclonal  
antibodies (Fig. 3c and Extended Data Fig. 4). Inhibition of reticulo-  
cyte binding to HEK293 cells expressing the constructs at their sur-  
face by anti-*PvRBP2a* antibodies was stronger than the inhibition  
observed with the anti-CD98 antibodies that target the reticulocyte  
surface. This might be due to differences in the affinities of the  
antibodies used, thereby leading to variable inhibitory efficiency.  
In addition, the exact regions of interaction between *PvRBP2a* and  
CD98 are still unknown. Thus, the different antibodies, despite  
their inhibitory effect, may not directly recognize the actual sites  
of interactions and thus provide optimal inhibition. Notably, one  
of these two antibodies also significantly inhibited the invasion  
of reticulocytes by *P. vivax* isolates (Fig. 3d). The moderate levels  
of inhibition observed could be due to genetic polymorphisms of  
*PvRBP2a* across *P. vivax* isolates (Supplementary Table 3) and/or  
low affinity of the two anti-*PvRBP2a* clones against the native pro-  
tein conformation(s).

To assess whether *PvRBP2a* and CD98 are direct binding part-  
ners, biochemical analyses were carried out. Immunoprecipitation  
of recombinant *PvRBP2a*<sub>160–1135</sub> was able to co-immunoprecipitate  
recombinant monomeric CD98 protein, which indicates that they  
are direct binding partners (Fig. 4a). Similarly, direct binding  
interactions were observed between *PvRBP2a* and CD98 by both  
ELISA and biolayer interferometry (Fig. 4a–d). We found that

118 **Fig. 1 | CD98, a trypsin-resistant protein, is specifically expressed on CD71<sup>+</sup> reticulocytes.** **a**, Schematic depicting the presence of an unknown *P. vivax*  
119 receptor involved in reticulocyte tropism (reticulocyte-specific receptor (RSR)). **b**, Comparison of protein abundance (expressed as relative fold-change)  
120 between CD71<sup>+</sup> reticulocytes and CD71<sup>-</sup> erythrocytes measured by MS (Supplementary Table 1). The “R” in blue denotes trypsin resistance (see also  
121 Extended Data Fig. 2). **c**, Flow cytometry profile of CD98 and CD71 expression on TO<sup>-</sup>, TO-low and TO-high erythrocytes for three different human cord  
122 blood samples. The TO-high subset represents the most immature reticulocyte population compared with the TO-low subset (<https://www.bdbiosciences.com/ds/is/tds/23-1789.pdf>). **d**, CD98 and Demantin (Band 4.9) expression in CD71<sup>-</sup> and CD71<sup>+</sup> erythrocytes (representative images are shown from an  
124 analysis consisting of 3 independent experiments, each time inspecting 40–50 cells), as recorded by immunofluorescence microscopy. Scale bar, 2 μm.  
125 **e**, Detection of CD98 by western blotting of ghost membranes derived from CD71<sup>-</sup> and CD71<sup>+</sup> erythrocytes matured ex vivo for 20 and 40 h. Band 3 anion  
126 exchange protein served as the loading control for western blots. Representative images are shown, and the pattern of CD98 expression was consistent  
127 as observed from a total of eight independent experiments, using three batches of blood **f**, Schematic representation of the CD98 structure (PDB access  
128 code: 6IRS) with the 4F2hc heavy-chain ectodomain of CD98 depicted as blue ribbons and its N-linked glycans as black sticks. The membrane-embedded  
129 light chain of CD98 (4F2lc) is depicted as yellow ribbons<sup>25</sup>.

monomeric CD98 interacted with PvRBP2a with a dissociation constant ( $K_D$ ) value of  $12.3 \pm 1.5$  nM at 37°C by ELISA using the method outlined in Friguet et al.<sup>29</sup> (Fig. 4c,d) and  $5.9 \pm 1.5$  nM at 37°C by biolayer interferometry. Notably, this interaction is stronger

than the first binding event of the canonical *P. vivax* invasion receptor, Duffy-binding protein (PvDBP) ( $K_D$  of  $2.2 \mu\text{M}$ )<sup>30</sup>, or the interaction between the *P. falciparum* invasion receptor PfRh4 and its cognate partner CR1 ( $K_D$  of  $2.9 \mu\text{M}$ )<sup>31</sup> (Supplementary Table 4).





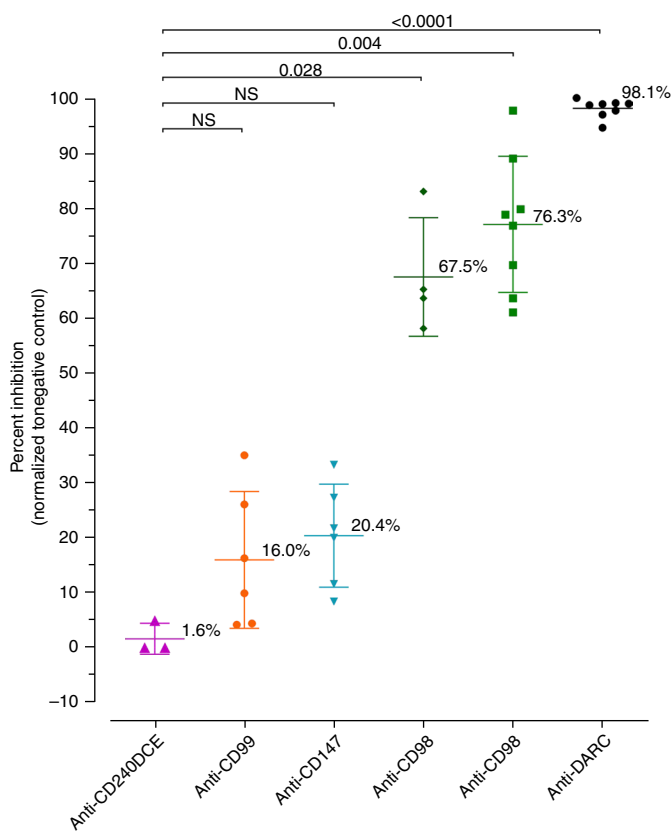


**Fig. 2 | CD98 is essential for *P. vivax* invasion.** *P. vivax* invasion inhibition assay in the presence of anti-CD240DCE (monoclonal), anti-CD99 (monoclonal), anti-CD147 (monoclonal), anti-CD98 (polyclonal) and anti-CD98 (monoclonal) F(ab')<sub>2</sub> antibodies (final concentration of 25 µg ml<sup>-1</sup>). The anti-DARC antibody (monoclonal) was used as an inhibition positive-control, and a total of eight *P. vivax* clinical isolates were used. Inhibition values are represented as the mean ± s.d., Kruskal-Wallis test ( $P < 0.0001$ ). NS, not significant.

196  
197  
198 The distinct tropism for different subsets of RBCs by *Plasmodium*  
199 parasites infecting humans as well as other mammalian hosts has  
200 held the interest of malariologists for more than 80 years. This was  
201 not for mere scientific curiosity, as the erythrocyte niche favoured  
202 by the parasite clearly has a major influence on the parasitologi-  
203 cal course and the clinical outcome of the infection. Restriction to  
204 reticulocytes could be considered a natural means to moderate par-  
205 asite burden and the consequent pathology, allowing both host and  
206 parasite survival. Indeed, in humans, clinical severity is less frequent  
207 in *P. vivax* than in *P. falciparum* malaria, for which the parasite  
208 invades all erythrocyte subsets. While the reticulocyte restriction  
209 has previously been postulated to be due to specific metabolic needs  
210 of *P. vivax* associated with a reticulocyte microenvironment<sup>32</sup> and  
211 bone marrow localization<sup>33</sup>, we present compelling evidence that  
212 reticulocyte restriction is also caused by invasion receptor tropism.  
213 Specifically, CD98 plays an important role as a reticulocyte-specific  
214 host receptor, and PvRBP2a was identified as its corresponding  
215 parasite ligand. PvRBP2a is a member of a multigene family of  
216 11 members<sup>5</sup>, some of which, like PvRBP2b, are involved in reticu-  
217 loyte invasion by *P. vivax*<sup>34,35</sup>. Interestingly, PvRBP2a can induce  
218 a strong immunoglobulin G response<sup>36</sup>. It now becomes important  
219 to determine whether the PvRBP2a–CD98 interaction is essential  
220 for reticulocyte recognition for all *P. vivax* populations. Indeed,  
221 the occurrence of alternative invasion pathways, known for *P. falciparum*,  
222 has recently been raised for *P. vivax* when infections by this parasite,  
once considered strictly Duffy-dependent, were recorded

in Duffy-negative individuals in Africa and South America<sup>37–39</sup>. PvRBP2a was also shown to bind to other unknown proteins present on normocytes and reticulocytes. Nonetheless, this was not sufficient to drive invasion of the mature RBCs. PvRBP2a–CD98 and PvRBP2b–CD71 can now be considered as two major ligand–receptor pairs implicated in the invasion of reticulocytes by *P. vivax*. The fact that one is trypsin-resistant and the other not, although apparently contradictory, might denote a combined interaction, a phenomenon of alternative invasion pathways or it might be due to a reliance on distinct receptors by different parasite strains. This can only be addressed by invasion inhibition assays in which identical parasite isolates (which are often polyclonal) are confronted head-to-head with the same sets of anti-CD71, anti-CD98 or anti-DARC antibodies. The current data only allow speculation on the nature of the contributions of CD98 versus that of CD71 in invasion, especially since these datasets relied on different host cell types for the invasion assays. It is interesting to note that indications for an alternative invasion pathway has been recently obtained using *P. vivax* isolates from India<sup>20</sup>. This, as well as the identification of other potential associations between PvRBPs and host receptors, merits further study, especially with respect to potential future vaccine development. Finally, the identification of reticulocyte-specific receptor–ligand pairs<sup>11</sup> could help the development of continuous in vitro culture of *P. vivax*, for example, by expressing specific receptors on normocytes allowing invasion; the current lack of such a tool is severely hampering research on this parasite. Ultimately, this provides the community with a vaccine candidate that could contribute to the control and eventual eradication of this globally important pathogen.

## Methods

**Ethics statement.** The clinical samples used in this study were collected from patients infected with *P. vivax* and from healthy donors (for the cord blood) attending the clinics of the Shoklo Malaria Research Unit (SMRU), Mae Sot, Thailand, under the following ethical guidelines in the approved protocols: OXTREC 45-09 and OXTREC 17–11 (University of Oxford, Centre for Clinical Vaccinology and Tropical Medicine, UK) and MUTM 2008–215 from the Ethics Committee of Faculty of Tropical Medicine, Mahidol University. Human cord blood and adult peripheral blood samples were collected under SingHealth CIRB 2019/2443- and 2017/2806-approved protocols, respectively, and written informed consent was obtained from participants.

**CD98 cloning and expression in Sf-9 cells.** The coding sequence of the soluble domain of CD98 (W218-A630) was cloned using the primers A 5'-TATCCACCTTTACTGTTAGGCCCGTAGG-3' and B 5'-TACTTCCAATCCATGTGGTGGCACACGGGC-3', and the amplified fragment was purified before insertion into a pFastBac-LIC-BseR1 (Addgene) plasmid using a Gibson Assembly Cloning kit (NEB). *Escherichia coli* Top10 competent cells were transformed with the ligated plasmid (pFastBac-CD98) and spread on LB plates supplemented with ampicillin. *E. coli* DH10Bac competent cells were transformed with the purified pFastBac-CD98 plasmid. Extraction of the bacmid and virus packaging was done according to Bac-to-Bac (Invitrogen). For expression, Sf-9 cells were infected at a multiplicity of infection of 1 for 72 h at 27 °C under agitation. Cells were collected at 3,000 × g for 15 min, and the cell pellet was stored at –20 °C.

**CD98 purification.** Cells were resuspended in 20 mM Tris pH 7.5, 500 mM NaCl and 10 mM imidazole and lysed by sonication. After centrifugation at 20,000 × g for 45 min, the filtered supernatant was injected into a nickel affinity column (HisTrap 1 ml, GE Healthcare). After a washing step of 6% of 20 mM Tris-HCl pH 7.5, 500 mM NaCl and 500 mM imidazole (buffer B), the protein was eluted with 100% of buffer B and injected into a Superdex 75 Hiload 26/60 gel-filtration column (GE Healthcare) equilibrated in PBS. The protein fractions were pooled and concentrated to 19 mg ml<sup>-1</sup> before being flash-frozen in liquid nitrogen and stored at –80 °C.

**Reticulocyte enrichment.** Enrichment of CD71<sup>+</sup> reticulocytes was performed using the MACS system (Miltenyi). A total of 1–2 ml of blood at 50% haematocrit in PBS was passed through a LS column. The purity of the positive and negative fractions was monitored by flow cytometry using thiazole orange (TO), which stains RNA (the only nucleic acid species present in reticulocytes) and used for routine clinical quantitation of reticulocytes (<https://wwwbdbiosciences.com/ds/is/tds/23-1789.pdf>). The purity of CD71<sup>+</sup> cells was >80%.

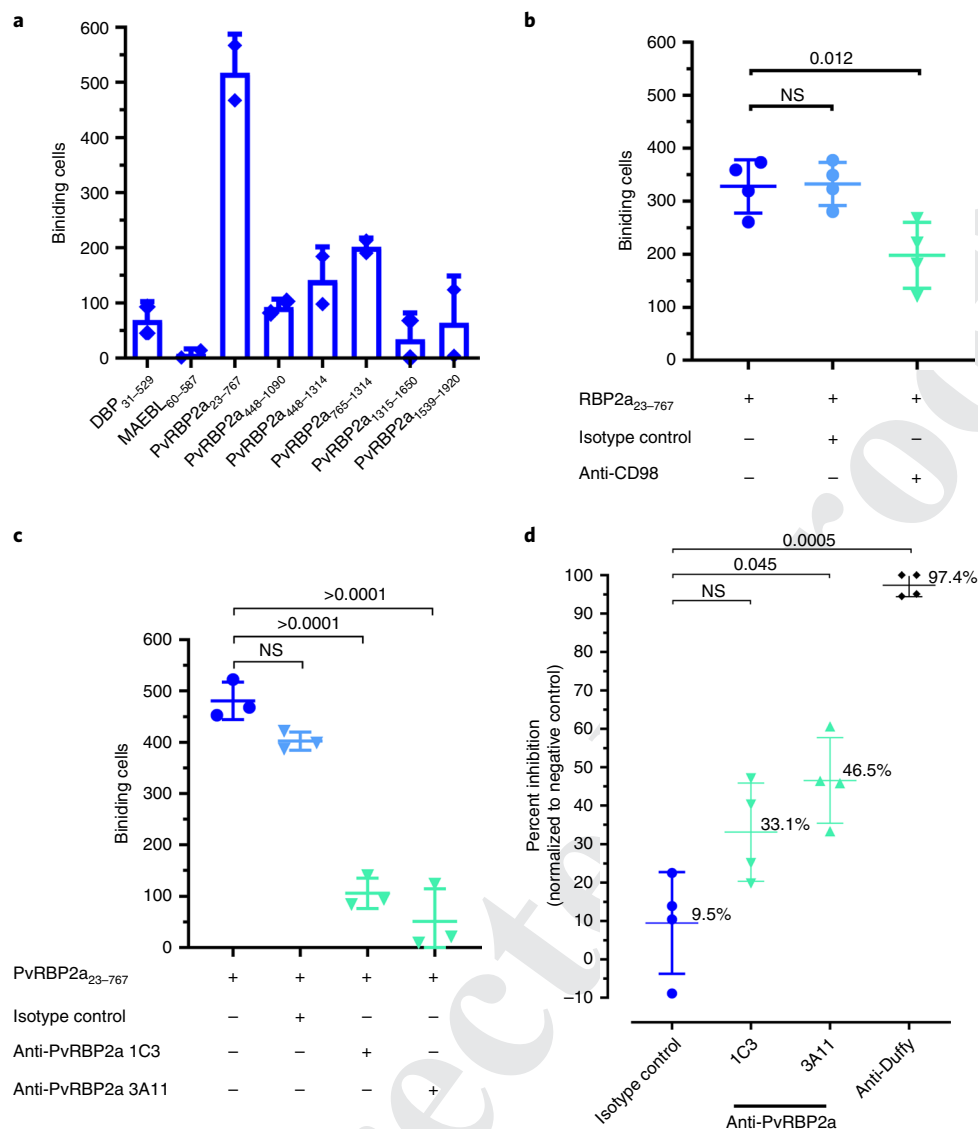


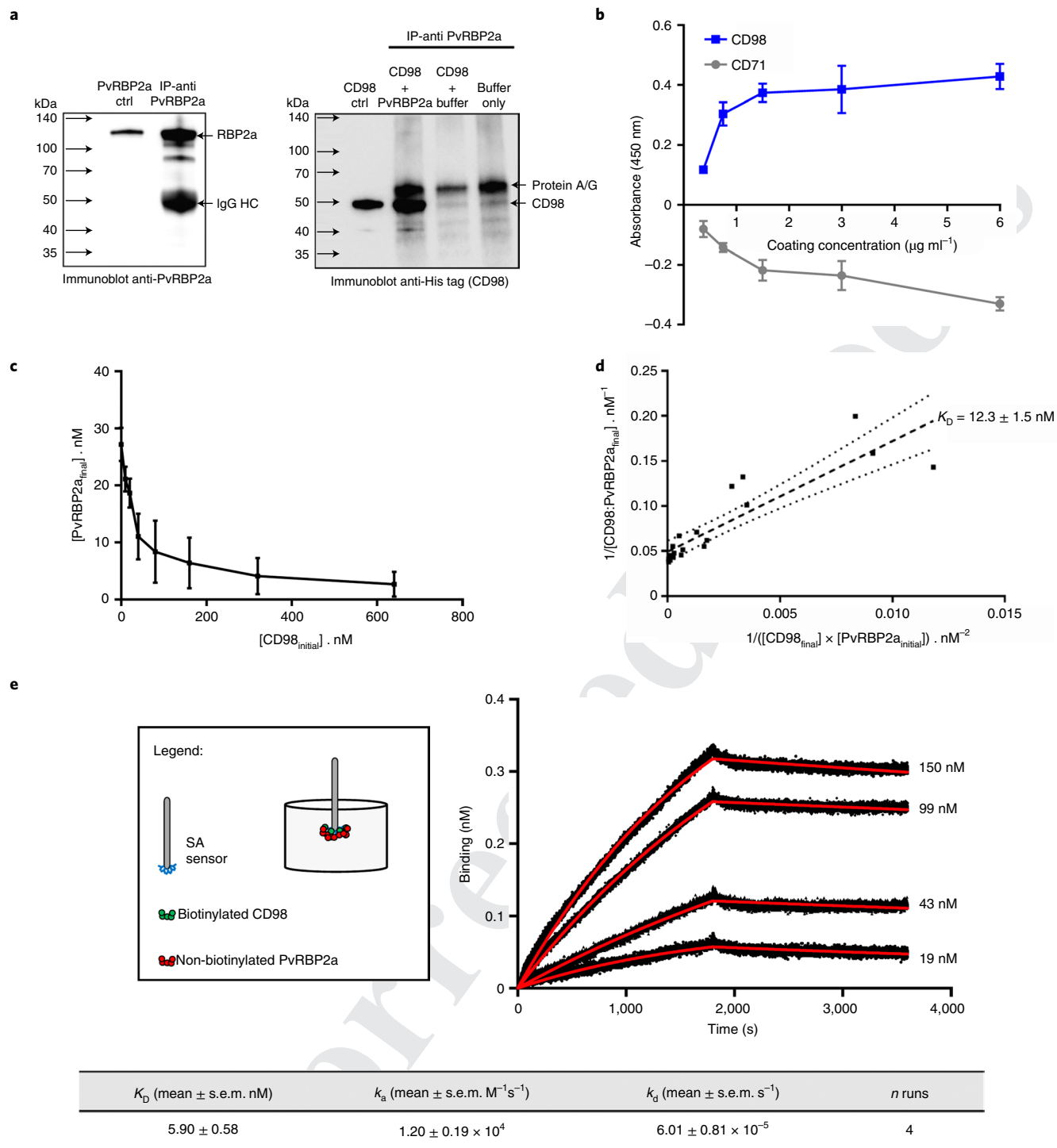
**Fig. 3 | PvrBP2a is important for *P. vivax* invasion.** **a**, Binding of reticulocytes to 1,000 HEK293 cells transfected (efficiency > 20%) with different gene or gene fragment from *P. vivax*. Binding was assessed for HEK293 cells expressing a fragment of Duffy binding protein II (DBP) known to contain an erythrocyte-binding domain<sup>40</sup> or different fragments of PvrBP2a (PvRBP2a<sub>23-767</sub>, PvRBP2a<sub>448-1090</sub>, PvRBP2a<sub>448-1314</sub>, PvRBP2a<sub>765-1314</sub>, PvRBP2a<sub>1315-1650</sub> or PvRBP2a<sub>1539-1920</sub>), or MAEBL<sub>60-587</sub>. Specific binding numbers to transfected HEK293 cells were determined after subtraction of the number of reticulocytes or normocytes binding to non-transfected HEK293 cells (screening was done in duplicate). **b**, Binding assays of reticulocytes to HEK293 cells expressing PvRBP2a<sub>23-767</sub> in the presence or absence of isotype control or anti-CD98 antibodies (concentrations). The binding of normocytes to HEK293 cells expressing PvRBP2a<sub>23-767</sub> was specific since the addition of antibodies against CD98 did not abrogate binding to normocytes (Extended Data Fig. 3c). Values are expressed as the mean  $\pm$  s.d., ANOVA followed by Dunnett post-test. **c**, Binding assays with reticulocytes in the presence of PvRBP2a<sub>23-767</sub> fragment and antibodies against RBP2a (1C3 and 3A11 at 25  $\mu$ g ml<sup>-1</sup>). Values are expressed as the mean  $\pm$  s.d., ANOVA followed by Dunnett post-test. **d**, Inhibition of *P. vivax* invasion using two different mouse monoclonal anti-PvrBP2a (1C3 and 3A11) antibodies and one anti-DARC antibody with four different isolates tested in parallel. The inhibition was normalized to invasion efficiencies obtained without antibodies. Values are expressed as the mean  $\pm$  s.d., Kruskal-Wallis test ( $P < 0.0001$ ).

**Sample preparation and quantitative mass spectrometry.** After MACS enrichment, samples were prepared and analysed on a mass spectrometer as described in Chu et al.<sup>21</sup>. Briefly, after isolation, both reticulocytes and normocytes were lysed using 0.02% saponin in PBS with protease inhibitors. Following this, the membrane and soluble fractions were separated by differential centrifugation and precipitated with ice-cold acetone. For the membrane fraction, the sample was reduced using 5 mM Tris 2-carboxy-ethyl phosphine hydrochloride for 3 h at 30°C and then alkylated in the dark using 55 mM iodoacetamide for 1 h at room temperature (RT). In-solution digestion of different protein samples with trypsin (Promega) was carried out (at 10 ng ml<sup>-1</sup> final concentration) at 37°C for 16 h. These samples were desalted and then labelled with isobaric tags as described in Chu et al.<sup>21</sup>, with ~95% labelling efficiency. We labelled CD71<sup>-</sup> membrane samples

with 116 isobaric tags and CD71<sup>+</sup> membrane samples with 117 isobaric tags. These samples were further fractionated using a X-Bridge C18 column (Waters; 4.6  $\times$  250 mm, 5  $\mu$ m, 300 Å). Fractions obtained from this LC step were analysed using an Ultimate 3000 RSLC nano-HPLC system (Dionex) coupled to a QExactive Hybrid Quadrupole-Orbitrap mass spectrometer (Thermo Scientific).

**Proteomics analysis. Database searching.** All tandem mass spectrometry (MS/MS) samples were analysed using Mascot (Matrix Science, v.2.4.1). Mascot was set up to search the con\_uni\_human\_20150401\_20150623 database (unknown version, 180,822 entries) assuming the digestion enzyme trypsin. Mascot was searched with a fragment ion mass tolerance of 0.020 Da and a parent ion tolerance of 10.0 ppm. Carbamidomethyl of cysteine and iTRAQ4plex of lysine and the amino terminus

289  
290  
291  
292  
293  
294  
295  
296  
297  
298  
299  
300  
301  
302  
303  
304  
305  
306  
307  
308  
309  
310  
311  
312  
313  
314  
315  
316  
317  
318  
319  
320  
321  
322  
323  
324  
325  
326  
327  
328  
329  
330  
331  
332  
333  
334  
335  
336  
337  
338  
339  
340  
341  
342  
343  
344  
345  
346  
347  
348  
349  
350  
351  
352  
353  
354



were specified in Mascot as fixed modifications. Deamidated asparagine and glutamine, oxidation of methionine and iTRAQ4plex of tyrosine were specified in Mascot as variable modifications.

**Criteria for protein identification.** Scaffold (v.Scaffold\_4.4.3, Proteome Software) was used to validate MS/MS-based peptide and protein identifications. Peptide identifications were accepted if they could be established at greater than 95.0% probability by the Peptide Prophet algorithm<sup>41</sup> with Scaffold delta-mass correction. Protein identifications were accepted if they could be established at greater than 99.0% probability and contained at least 2 identified peptides. Protein probabilities were assigned by the Protein Prophet algorithm<sup>42</sup>. The original MS dataset (as published by Chu et al.<sup>21</sup>) is available at Proteome Xchange Consortium via the PRIDE partner repository with the identifier [PXD003851](https://www.ebi.ac.uk/pride/archive/projects/PXD003851) (Supplementary Dataset 2).

**Flow cytometry phenotyping of cord blood samples and HEK293 cells expressing RBP2a<sub>23-767</sub>.** Three Percoll-enriched reticulocyte samples from human cord blood were treated or not with trypsin (1 mg ml<sup>-1</sup>; Sigma)<sup>28</sup>. Packed cord blood (500 nL, 47.4  $\pm$  14.5% CD71<sup>+</sup>,  $n = 3$ ) was stained with different mouse anti-human marker antibodies followed by a F(ab')<sub>2</sub> anti-mouse immunoglobulin antibody coupled to eFluor 660 (eBioscience)<sup>12</sup>. The antibodies used in this study are described in Supplementary Table 5. Fifty thousand events were acquired on a LSR II flow cytometer (BD Biosciences) for each sample, and the data were analysed using FlowJo software (Three Star).

HEK293 cells expressing RBP2a<sub>23-767</sub> were stained with two mouse anti-PVRBP2a monoclonal antibodies (1C3 and 3A11) at 25  $\mu$ g ml<sup>-1</sup> followed by a (Fab')<sub>2</sub> anti-mouse immunoglobulin antibody coupled to eFluor 660 (eBioscience) or with anti-Myc (Miltenyi Biotec) antibodies followed by a (Fab')<sub>2</sub> anti-rabbit immunoglobulin antibody coupled to Alexa 647 (Invitrogen).

**Fig. 4 | PvRBP2a interacts with CD98.** **a**, Recombinant His-tagged CD98 was incubated with PvRBP2a for 2 h at 37 °C. PvRBP2a was then immunoprecipitated with rabbit anti-PvRBP2a-bound protein A/G magnetic beads. Left: lane 1 shows 75 ng of recombinant PvRBP2a as a positive control, lane 2 shows successful immunoprecipitation (IP) of PvRBP2a. Right: lane 1 shows 75 ng of CD98 as a positive control, lane 2 shows successful immunoprecipitation of CD98 from PvRBP2a mixed with CD98, lanes 3 and 4 are controls using anti-PvRBP2a-bound beads incubated with CD98 without PvRBP2a, or beads alone, respectively. Protein ladder size inferred from the colorimetric images are indicated on chemiluminescent image panels (representative images from three independent experiments). **b**, Binding of PvRBP2a to CD98 or CD71 proteins coated on an ELISA plate. A total of 25 µg ml<sup>-1</sup> PvRBP2a was added to plates pre-coated with 0–6 µg ml<sup>-1</sup> of CD98 or CD71. Excess PvRBP2a was washed off, and bound PvRBP2a was detected using a rabbit anti-PvRBP2a antibody, followed by a goat anti-rabbit HRP-conjugated secondary antibody. Background-subtracted optical density values relative to an uncoated control are reported. Error bars indicate the standard deviation from two technical replicates within a representative experiment of two independent experiments. **c**, PvRBP2a and various concentrations of CD98 ([CD98]<sub>initial</sub>) were pre-incubated in solution for 2.5 h at 37 °C for binding to reach equilibrium. After the incubation time, the solution was applied to plates pre-coated with CD98 to detect the remaining unbound PvRBP2a concentration ([PvRBP2a]<sub>final</sub>). Error bars indicate the standard deviation of three independent experiments. **d**, Klotz plot of the binding of PvRBP2a to CD98, where the  $K_D$  was derived from the slope of the best-fit line<sup>29</sup>. Data from three independent experiments are shown. **e**, Left: representative binding sensorgram showing the binding of non-biotinylated PvRBP2a to 25 nM biotinylated CD98 in a dose-dependent manner. The binding of PvRBP2a to CD98 was detected using the Octet Red 96e biolayer interferometry system. Biotinylated CD98 was loaded onto the streptavidin (SA) sensor followed by dipping into wells containing the indicated concentration of PvRBP2a. Right: the real-time binding curves are shown as black lines while the red lines indicate the global fits generated using 1:1 Langmuir binding model.

**Profiling CD98 expression on RBCs by western blotting.** Immature reticulocytes (CD71<sup>+</sup>) were purified from cord blood using magnetic beads conjugated to anti-CD71 antibody using the MACS purification system (Miltenyi Biotec). Purified CD71<sup>+</sup> cells were allowed to mature *ex vivo* in RPMI medium supplemented with 5% Albumax at 37 °C. Aliquots of 3 µl packed cells were collected at different time points (0, 20 and 40 h). Cells were incubated with 40 volumes of 5 mM sodium phosphate for 10 min on ice with occasional gentle mixing, which induces membrane breaks and release of the cell cytoplasmic contents. The lysate was then centrifuged at 16,000 × g for 10 min at 4 °C to sediment the RBC ghosts that were again washed twice in ice-cold 5 mM sodium phosphate.

Purified ghost membranes were treated with 0.25% Triton X-100/PBS. Membrane extracts corresponding to 10 µg total protein (estimated using a BCA assay) obtained at different time points during reticulocyte maturation, together with a normocyte membrane sample that was prepared alongside, were extracted in reduced Laemmli buffer, incubated at 37 °C for 10 min, then resolved by 10% SDS-PAGE and transferred to polyvinylidene difluoride membrane. Samples were probed using anti-CD98 antibody (E-5: sc-376815, Santa Cruz Biotechnology) at 1:500 dilution in PBS followed by a mouse secondary antibody conjugated to horseradish peroxidase (HRP) and visualized by ECL detection (Thermo Fisher Scientific). An antibody against Band-3 anion exchanger was used for loading control.

**Immunofluorescence assay.** RBCs (CD71<sup>+</sup> and CD71<sup>-</sup>) were fixed in 4% paraformaldehyde (Sigma Aldrich) and 0.0075% glutaraldehyde (Sigma Aldrich) in PBS for 30 min at RT. Subsequently, cells were washed in 1 × PBS, quenched in 0.125 M glycine/PBS for 15 min at RT, washed again and permeabilized in 0.1% Triton X-100/PBS for 10 min at RT. After blocking for 1 h in blocking solution (3% BSA (w/v) in PBS), samples were incubated with rabbit anti-CD98 antibody (EPR3548 clone, Abcam) or rabbit anti-Dematrin (Band 4.9) antibody (Thermo Fisher Scientific) both at a 1:100 dilution, for 1 h, followed by Alexa Fluor<sup>®</sup> 546-conjugated anti-rabbit secondary antibodies (1:200; Invitrogen). Images were acquired with a Zeiss LSM 700 microscope (Carl Zeiss) using a ×63/1.4 oil DIC objective lens. Images were processed using LSM software Zen 2009 (Carl Zeiss).

***P. vivax* parasite collection and cryopreservation.** *P. vivax*-infected blood samples were collected from patients with malaria receiving treatment at clinics run by the SMRU located at the north-western border of Thailand. The project was explained to all the patients before they provided informed consent before collection of blood by venepuncture. Whole blood (5 ml) was collected in lithium heparin collection tubes. These samples were cryopreserved in Glycerolyte 57 (Baxter) after leukocyte depletion using cellulose columns (Sigma, C6288)<sup>43</sup>. After thawing, the parasites present in the packed cells (1.5 ml per isolate) were cultured to the schizont stage in 12 ml of McCoy 5A medium supplemented with 2.4 g per litre D-glucose and 20% heat-inactivated human AB serum, in 5% O<sub>2</sub> at 37.5 °C<sup>4</sup>.

***P. vivax* invasion assay.** Invasion assays using freshly isolated *P. vivax* field samples were performed as previously described<sup>28</sup>. In some experiments, anti-human CD147 (BD Bioscience, clone HIM6), CD240DCE (AbD Serotec, clone BRIC 69), polyclonal CD98 (TransGenic), monoclonal CD98 (BD Bioscience, clone UM7F8) and anti-DARC (Fy6)<sup>44</sup> F(ab')<sub>2</sub> antibodies were added. The antibodies were prepared using a Pierce Fab Micro Preparation kit (ThermoScientific Pierce) as previously described<sup>45</sup>. We chose to use F(ab')<sub>2</sub> antibodies to avoid steric hindrance or agglutination of erythrocytes. All antibodies were diluted in PBS and were azide- and glycerol-free. Concentrated mature schizont preparations were mixed with the CD71<sup>+</sup> reticulocyte-enriched fraction and pre-incubated for 10 min with

each antibody (final concentration of 25 µg ml<sup>-1</sup>)<sup>28</sup>. After 24 h of culture at 37 °C, blood thin smears were made and stained with Giemsa (Sigma-Aldrich). One to five thousand erythrocytes were counted per slide, and the lowest parasitaemia was 0.3% for the negative control (no monoclonal antibody) condition used to normalize the invasion assays.

The anti-human CD147 (BD Bioscience, clone HIM6) abrogated the invasion of three *P. falciparum* samples (one field isolate and two clones) with an efficiency of 87.6 ± 2.4% and 86.0 ± 5.4% in CD71<sup>-</sup> and CD71<sup>+</sup> reticulocytes, respectively.

***P. vivax* antigen library.** The *P. vivax* antigen library was designed and established as previously described for a *P. falciparum* library<sup>46</sup> using *P. vivax* UMS203 as the template. Briefly, 28 gene fragments corresponding to 7 different *P. vivax* genes were amplified using PCR and either *P. vivax* genomic DNA or RNA as template, and cloned into the pDisplay vector (Invitrogen) (Supplementary Table 2). Cloning of PvRBP2a,b,c into expression vector codon-optimized DNA of PvRBP2a,b,c was purchased from Genscript. The resultant plasmids were then transfected into HEK293 cells using Lipofectamine 2000 (Invitrogen) for surface expression of the *P. vivax* antigens. The *P. vivax* antigens were tagged with a haemagglutinin (HA) short sequence at the N-terminal and a Myc short sequence at the carboxy-terminal part of the protein. These tags allow the assessment of transfection efficacy and expression level of the *P. vivax* antigen using an anti-HA (Sigma) or anti-Myc (Miltenyi Biotec) antibodies. Only HEK293 cells expressing *P. vivax* genes with transfection efficiency >20% were used. The PvRBP2a diversity is compiled in Supplementary Table 3.

**Erythrocyte binding assay using the *P. vivax* antigen library.** Adherent HEK293 cells transfected with *P. vivax* antigens were incubated with CD71<sup>+</sup> or CD71<sup>-</sup> erythrocytes loaded with carboxy-fluorescein diacetate succinimidyl ester (CFSE) for 1 h at 37 °C under agitation. After five washing steps using PBS, cell binding was recorded using a confocal microscope. One thousand HEK293 cells were counted at ×40 magnification, and each CFSE-stained erythrocyte in contact with HEK293 cells were counted as a binding cell using the software IMARIS (Bitplane). For each experiment, the number of erythrocytes binding untransfected HEK293 cells was subtracted.

Reticulocyte binding inhibition and the competition assay were conducted by incubating the PvRBP2a-transfected HEK293 cells before adding reticulocytes with an isotype control anti-TNP (BD Bioscience, clone A111-3) and two different mouse anti-PvRBP2a antibodies (clone1C3 and 3A11, described below) or mouse anti-CD98 monoclonal antibody (BD Bioscience, clone UM7F8) and mouse anti-human CD147 (BD Bioscience, clone HIM6) at 25 µg ml<sup>-1</sup> in PBS.

**Anti-PvRBP2a mouse monoclonal antibody production.** Anti-PvRBP2a monoclonal antibodies were produced at the Monoclonal Antibody Facility at the Walter and Eliza Hall Institute. BALB/c and C57BL/6 mice received three immunizations of recombinant PvRBP2a<sub>160–1135</sub> purified as previously described<sup>45</sup>. At day 0, complete Freund adjuvant was mixed with the antigen into an emulsion and intraperitoneally injected. At days 30 and 60, the antigen was mixed with incomplete Freund adjuvant, and the resulting emulsion intraperitoneally injected. Serum samples were taken at day 72 and ELISAs were performed using the same recombinant protein. The mouse with the best response received a final injection of antigen in saline, and splenocytes were collected 3 days later. Spleen cells were fused with SP2/0 myeloma cells to generate hybridomas. Hybridomas were grown in hypoxanthine-aminopterin thymidine growth medium. ELISA was used to select hybridomas producing antibodies specific to PvRBP2a. Hybridomas were cloned by limiting dilution in multwell plates aiming for one cell or fewer per well. The subcloning supernatants were screened by ELISA. Two or more rounds



of limiting dilution cloning were generally required before the hybridomas were deemed monoclonal. The antibodies were purified from monoclonal hybridoma supernatants with protein A sepharose.

**ELISA-based binding assay between PvRBP2a and CD98.** To examine the binding between PvRBP2a<sub>233-767</sub> and CD98 recombinant protein, Maxisorp plates were coated with 3 µg ml<sup>-1</sup> CD98 or BSA in 0.1 M sodium bicarbonate buffer (pH 9.6) overnight at 4 °C. Plates were then blocked with 5% BSA in 0.05% PBST (PBS buffer supplemented with Tween-20) for 1.5 h at 37 °C. PvRBP2a in 0.5% BSA/0.05% PBST was then added at varying concentrations from 0 nM to 50 nM and incubated for 1 h at 37 °C. To detect the quantity of bound PvRBP2a, rabbit anti-PvRBP2a antibody was added and incubated for 1 h at 37 °C, followed by a secondary goat anti-rabbit HRP-conjugated antibody, with a colorimetric TMB substrate-based readout.

**ELISA-based solution binding  $K_D$  between PvRBP2a and CD98.** The  $K_D$  of binding between PvRBP2a and CD98 was quantified using the method outlined in Friguet et al.<sup>29</sup>. PvRBP2a (25 nM) and CD98 (0 nM to 640 nM) were pre-incubated in solution for binding to occur. The duration of pre-incubation was optimized to 2.5 h at 37 °C to allow maximal time for the binding reaction to reach equilibrium while minimizing protein degradation. After the incubation time, the solution was applied to plates pre-coated with 3 µg ml<sup>-1</sup> CD98 and blocked with 5% BSA/0.05% PBST, followed by secondary detection with rabbit anti-PvRBP2a and goat anti-rabbit HRP antibodies as described above. Resulting optical density values were transformed to molar PvRBP2a concentrations by normalization to a set of standards run in parallel. This gave the concentration of unbound PvRBP2a at equilibrium ([PvRBP2a<sub>final</sub>]), assuming that the PvRBP2a already bound to solution-phase CD98 cannot bind to the plate-coated CD98. For each mixture of PvRBP2a and CD98, the concentration of PvRBP2a bound by CD98 in solution during the pre-incubation phase ([CD98:PvRBP2a<sub>final</sub>]) was calculated as the difference between its concentration of unbound PvRBP2a ([PvRBP2a<sub>final</sub>]) and the PvRBP2a concentration of a control well with the same input PvRBP2a concentration and pre-incubation conditions but which contained no CD98 ([PvRBP2a<sub>initial</sub>]). The final concentration of CD98 at equilibrium, [CD98<sub>final</sub>], was calculated by subtracting the concentration of bound CD98 ([CD98:PvRBP2a<sub>final</sub>]) from the initial known input concentration of CD98 ([CD98<sub>initial</sub>]). With these values, the  $K_D$ , which for a 1:1 binding relationship is defined as [PvRBP2a<sub>final</sub>][CD98<sub>final</sub>]/[CD98:PvRBP2a<sub>final</sub>], can be calculated. Since the equation for  $K_D$  can be rewritten as  $1/[CD98:PvRBP2a_{final}] = K_D \times 1/([CD98_{final}] \times [PvRBP2a_{initial}]) + 1/[PvRBP2a_{initial}]$ , which is in the linear equation format  $y = mx + b$ , the gradient of the best fit line when plotting  $1/[CD98:PvRBP2a_{final}]$  against  $1/([CD98_{final}] \times [PvRBP2a_{initial}])$  shows the observed  $K_D$  across varying ratios of input PvRBP2a and CD98 concentrations.

**Kinetic binding assay using the Octet Red96e system.** Binding sensorgrams were collected using eight-channel detection mode on the Octet Red 96e system. Fresh streptavidin sensors were used without any regeneration step. The streptavidin sensor, without biotinylated CD98 loading, was used as the reference. Kinetic binding assays were performed using Octet Data Acquisition (v.10.0.1.3) at 37 °C with the orbital shaking speed set at 1,000 r.p.m. The assay was carried out in PBS buffer supplemented with 0.05% Tween-20 and 1 mg ml<sup>-1</sup> BSA (PBST/BSA). The biosensor was sequentially dipped into wells containing 200 µl each of the following solution: (1) baseline, PBST/BSA (60 s); (2) loading, 25 nM biotinylated CD98 (5 min); (3) washing, PBST/BSA (60 s); (4) blocking, 25 µM biocytin (5 min) to minimize nonspecific binding of PvRBP2a to the sensor; (5) washing, PBST/BSA (60 s); (6) association, varying concentrations of non-biotinylated P9 (30 min); and (7) dissociation, PBST/BSA (30 min). Binding sensorgrams were analysed using ForteBio's Data Analysis (v.10.0). All sensorgrams were subtracted to the reference sensor and aligned to the baseline. The sensorgrams were globally fit to a 1:1 Langmuir binding model. Association ( $k_a$ , M<sup>-1</sup> s<sup>-1</sup>), dissociation ( $k_d$ , s<sup>-1</sup>) and affinity constants ( $K_D$ , nM) were calculated based on quadruplicate runs and represented as mean ± s.e.m.

**Immunoprecipitation of full-length PvRBP2a.** A total of 25 µg of PvRBP2a<sub>233-767</sub> and His-tagged CD98 or His-tagged CD98 alone were incubated at 37 °C for 2 h in IP buffer 1 (50 mM Tris HCl pH 7.5, 1% Triton and 150 mM NaCl). In parallel, 100 µl of protein A/G magnetic beads (Pierce, 88802) were washed with IP buffer 1 and incubated at RT with 20 µg of anti-PvRBP2a<sup>11</sup>. Beads were then washed three times before incubating for 1 h at 37 °C with lysis buffer 1 alone or with lysis buffer 1 containing CD98 or CD98 and PvRBP2a<sub>233-767</sub>. Beads were then washed four times with IP buffer 2 (50 mM Tris HCl pH 7.5 (Gibco), 1% IGEPAL (Sigma), 0.5% sodium deoxycholate (Sigma) and 150 mM NaCl (Ambion)). This was followed by two washes with tube change in 50 mM Tris HCl to avoid nonspecific carry over, and elution in 1× Laemmli buffer (Bio-Rad) with β-mercaptoethanol (Sigma) and boiling for 5–10 min before western blotting was performed as described in Carissimo et al.<sup>47</sup>. Briefly, samples were deposited on 4–15% or 4–20% TGX mini-protein gels (Bio-Rad), with Spectra BR (ThermoFisher) used as a protein ladder, and ran in Bis-Tris buffer (Bio-Rad) at 120 V, and transferred to nitrocellulose membrane (Bio-Rad) using a semi-dry system and Bjerrum

Schafer–Nielsen buffer (48 mM UltraPure Tris (Invitrogen), 38 mM glycine (Bio-Rad) and 20% (v/v) EMSURE methanol (EMD Millipore)). Membranes were then blocked in 5% (w/v) non-fat milk powder (Nacalai Tesque) in 1× Tris buffer saline (first base) with Tween 0.1% (v/v) (Sigma) (TBST) for 1 h before staining in blocking buffer. Antibodies used for staining were anti-His-HRP (Sigma Aldrich) at 1:10,000 dilution to detect His-tagged CD98, anti-PvRBP2a<sup>11</sup> at 1:5,000 dilution and protein A/G-HRP (Pierce, 32490) at 1:15,000 dilution. Revelation was performed after membrane washing in 1× TBST using WesternBright ECL HRP substrate (Advanta), and the signal was acquired as multichannel (chemiluminescence and colorimetric) on a ChemiDoc screen touch model 2017 (Bio-Rad). Non-saturated images were analysed using ImageLab 2.3 software (Bio-Rad) and exported in TIFF format. Arrows indicated the protein ladder were added to the chemiluminescent images and then the resulting image was copied and incorporated in Illustrator (v.16.0.0, Adobe) to produce the figure panel. No brightness or contrast correction was applied to the images. Untouched full-size membrane images of the merged channels are provided in the source data. Experiments were performed three times independently and representative results are presented.

**Statistical analysis.** Nonparametric Kruskal–Wallis test followed by Dunn's post-test was used for the invasion inhibition assays (Fig. 2a), as the percentage of infected reticulocytes is not normally distributed<sup>29</sup>. For the difference in geometric mean (log-normalized data) fluorescence intensity (MFI), unpaired Student *t*-test was used (Extended Data Fig. 2c). D'Agostino's *K*-squared test was used to determine the normal distribution of reticulocyte binding assay data (Extended Data Fig. 3d) and unpaired Student *t*-test for the comparison between transfected and non-transfected HEK293 cells assuming unequal variances of the data (Fig. 3b,c). One-way analysis of variance (ANOVA) with Geisser–Greenhouse correction (variance not equal) followed by Tukey post-test was used for the comparison of reticulocyte binding to HEK293-transfected cells with isotype control or anti-PvRBP2a antibodies (Fig. 3d). All statistical analyses used Graph Pad Prism (7.0).

**Reporting Summary.** Further information on research design is available in the Nature Research Reporting Summary linked to this article.

## Data availability

Source data are provided with this paper. All data are available from the corresponding authors upon reasonable request.

Received: 5 December 2020; Accepted: 18 June 2021;

## References

1. *Confronting Plasmodium vivax malaria*. WHO/HTM/GMP/2015.3 (World Health Organization, 2015).
2. Hegner, R. Relative frequency of ring-stage plasmodia in reticulocytes and mature erythrocytes in man and monkey. *Am. J. Trop. Med. Hyg.* **27**, 690–718 (1938).
3. Mons, B., Croon, J. J., van der Star, W. & van der Kaay, H. J. Erythrocytic schizogony and invasion of *Plasmodium vivax* in vitro. *Int. J. Parasitol.* **18**, 307–311 (1988).
4. Malleret, B. et al. *Plasmodium vivax*: restricted tropism and rapid remodeling of CD71-positive reticulocytes. *Blood* **125**, 1314–1324 (2015).
5. Hester, J. et al. De novo assembly of a field isolate genome reveals novel *Plasmodium vivax* erythrocyte invasion genes. *PLoS Negl. Trop. Dis.* **7**, e2569 (2013).
6. Carlton, J. M. et al. Comparative genomics of the neglected human malaria parasite *Plasmodium vivax*. *Nature* **455**, 757–763 (2008).
7. Han, J. H. et al. Identification of a reticulocyte-specific binding domain of *Plasmodium vivax* reticulocyte-binding protein 1 that is homologous to the PfRh4 erythrocyte-binding domain. *Sci. Rep.* **6**, 26993 (2016).
8. Gupta, S. et al. Targeting a reticulocyte binding protein and Duffy binding protein to inhibit reticulocyte invasion by *Plasmodium vivax*. *Sci. Rep.* **8**, 10511 (2018).
9. Ntumngia, F. B. et al. Identification and immunological characterization of the ligand domain of *Plasmodium vivax* reticulocyte binding protein 1a. *J. Infect. Dis.* **218**, 1110–1118 (2018).
10. Chim-Ong, A. et al. The blood stage antigen RBP2-P1 of *Plasmodium vivax* binds reticulocytes and is a target of naturally acquired immunity. *Infect. Immun.* **88**, e00616–e00619 (2020).
11. Gruszczynk, J. et al. Transferrin receptor 1 is a reticulocyte-specific receptor for *Plasmodium vivax*. *Science* **359**, 48–55 (2018).
12. Malleret, B. et al. Significant biochemical, biophysical and metabolic diversity in circulating human cord blood reticulocytes. *PLoS ONE* **8**, e76062 (2013).
13. Proto, W. R. et al. Adaptation of *Plasmodium falciparum* to humans involved the loss of an ape-specific erythrocyte invasion ligand. *Nat. Commun.* **10**, 4512 (2019).

- 487 14. Kosaisavee, V. et al. Strict tropism for CD71+/CD234+ human reticulocytes  
488 limits the zoonotic potential of *Plasmodium cynomolgi*. *Blood* **130**, 1357–1363  
489 (2017).
- 490 15. Wright, G. J. & Rayner, J. C. *Plasmodium falciparum* erythrocyte invasion:  
491 combining function with immune evasion. *PLoS Pathog.* **10**, e1003943 (2014).
- 492 16. Crosnier, C. et al. Basigin is a receptor essential for erythrocyte invasion by  
493 *Plasmodium falciparum*. *Nature* **480**, 534–537 (2011).
- 494 17. Douglas, A. D. et al. Neutralization of *Plasmodium falciparum* merozoites by  
495 antibodies against PfrH5. *J. Immunol.* **192**, 245–258 (2014).
- 496 18. Barnwell, J. W., Nichols, M. E. & Rubinstein, P. In vitro evaluation of the  
497 role of the Duffy blood group in erythrocyte invasion by *Plasmodium vivax*.  
498 *J. Exp. Med.* **169**, 1795–1802 (1989).
- 499 19. Malleret, B., Renia, L. & Russell, B. The unhealthy attraction of *Plasmodium*  
500 *vivax* to reticulocytes expressing transferrin receptor 1 (CD71). *Int. J.*  
501 *Parasitol.* **47**, 379–383 (2017).
- 502 20. Kanjee, U. et al. *Plasmodium vivax* strains use alternative pathways for  
503 invasion. *J. Infect. Dis.* **223**, 1817–1821 (2020).
- 504 21. Chu, T. T. T. et al. Quantitative mass spectrometry of human reticulocytes  
505 reveal proteome-wide modifications during maturation. *Br. J. Haematol.* **180**,  
506 118–133 (2018).
- 507 22. Boado, R. J., Li, J. Y., Nagaya, M., Zhang, C. & Pardridge, W. M. Selective  
508 expression of the large neutral amino acid transporter at the blood–brain  
509 barrier. *Proc. Natl Acad. Sci. USA* **96**, 12079–12084 (1999).
- 510 23. Segawa, H. et al. Identification and functional characterization of a  
511 Na<sup>+</sup>-independent neutral amino acid transporter with broad substrate  
512 selectivity. *J. Biol. Chem.* **274**, 19745–19751 (1999).
- 513 24. Fort, J. et al. The structure of human 4F2hc ectodomain provides a model  
514 for homodimerization and electrostatic interaction with plasma membrane.  
515 *J. Biol. Chem.* **282**, 31444–31452 (2007).
- 516 25. Yan, R., Zhao, X., Lei, J. & Zhou, Q. Structure of the human LAT1-4F2hc  
517 heteromeric amino acid transporter complex. *Nature* **568**, 127–130 (2019).
- 518 26. Chiduzha, G. N. et al. LAT1 (SLC7A5) and CD98hc (SLC3A2) complex  
519 dynamics revealed by single-particle cryo-EM. *Acta Crystallogr. D Struct. Biol.*  
520 **75**, 660–669 (2019).
- 521 27. Lee, Y. et al. Cryo-EM structure of the human L-type amino acid transporter  
522 1 in complex with glycoprotein CD98hc. *Nat. Struct. Mol. Biol.* **26**, 510–517  
523 (2019).
- 524 28. Russell, B. et al. A reliable ex vivo invasion assay of human reticulocytes by  
525 *Plasmodium vivax*. *Blood* **118**, e74–e81 (2011).
- 526 29. Friguet, B., Chaffotte, A. F., Djavadi-Ohanian, L. & Goldberg, M. E.  
527 Measurements of the true affinity constant in solution of antigen–antibody  
528 complexes by enzyme-linked immunosorbent assay. *J. Immunol. Methods* **77**,  
529 305–319 (1985).
- 530 30. Batchelor, J. D. et al. Red blood cell invasion by *Plasmodium vivax*:  
531 structural basis for DBP engagement of DARC. *PLoS Pathog.* **10**, e1003869  
532 (2014).
- 533 31. Tham, W. H. et al. Complement receptor 1 is the host erythrocyte receptor  
534 for *Plasmodium falciparum* PfrH4 invasion ligand. *Proc. Natl Acad. Sci. USA*  
535 **107**, 17327–17332 (2010).
- 536 32. Srivastava, A. et al. Host reticulocytes provide metabolic reservoirs that can  
537 be exploited by malaria parasites. *PLoS Pathog.* **11**, e1004882 (2015).
- 538 33. Obaldia, N. III et al. Bone marrow is a major parasite reservoir in  
539 *Plasmodium vivax* infection. *mBio* **9**, e00625-18 (2018).
- 540 34. Galinski, M. R., Medina, C. C., Ingravallo, P. & Barnwell, J. W. A  
541 reticulocyte-binding protein complex of *Plasmodium vivax* merozoites. *Cell*  
542 **69**, 1213–1226 (1992).
- 543 35. Gruszczyk, J. et al. Structurally conserved erythrocyte-binding domain in  
544 *Plasmodium* provides a versatile scaffold for alternate receptor engagement.  
545 *Proc. Natl Acad. Sci. USA* **113**, E191–E200 (2016).
- 546 36. Franca, C. T. et al. *Plasmodium vivax* reticulocyte binding proteins are key  
547 targets of naturally acquired immunity in young Papua New Guinean  
548 children. *PLoS Negl. Trop. Dis.* **10**, e0005014 (2016).
- 549 37. Ryan, J. R. et al. Evidence for transmission of *Plasmodium vivax* among a  
550 Duffy antigen negative population in Western Kenya. *Am. J. Trop. Med. Hyg.*  
551 **75**, 575–581 (2006).
- 552 38. Menard, D. et al. *Plasmodium vivax* clinical malaria is commonly observed in  
553 Duffy-negative Malagasy people. *Proc. Natl Acad. Sci. USA* **107**, 5967–5971  
554 (2010).
- 555 39. Cavasini, C. E. et al. *Plasmodium vivax* infection among Duffy  
556 antigen-negative individuals from the Brazilian Amazon region: an exception?  
557 *Trans. R. Soc. Trop. Med. Hyg.* **101**, 1042–1044 (2007).
- 558 40. Chitnis, C. E. & Miller, L. H. Identification of the erythrocyte binding  
559 domains of *Plasmodium vivax* and *Plasmodium knowlesi* proteins involved in  
560 erythrocyte invasion. *J. Exp. Med.* **180**, 497–506 (1994).
41. Keller, A., Nesvizhskii, A. I., Kolker, E. & Aebersold, R. Empirical statistical  
model to estimate the accuracy of peptide identifications made by MS/MS  
and database search. *Anal. Chem.* **74**, 5383–5392 (2002).
42. Nesvizhskii, A. I., Keller, A., Kolker, E. & Aebersold, R. A statistical model  
for identifying proteins by tandem mass spectrometry. *Anal. Chem.* **75**,  
4646–4658 (2003).
43. Sriprawat, K. et al. Effective and cheap removal of leukocytes and platelets  
from *Plasmodium vivax* infected blood. *Malar. J.* **8**, 115 (2009).
44. Wasniowska, K. et al. Structural characterization of the epitope recognized by  
the new anti-Fy6 monoclonal antibody NaM 185-2C3. *Transfus. Med* **12**,  
205–211 (2002).
45. Lee, W. C. et al. Glycophorin C (CD236R) mediates vivax malaria parasite  
rosetting to normocytes. *Blood* **123**, e100–e109 (2014).
46. Peng, K. et al. Breadth of humoral response and antigenic targets of  
sporoziite-inhibitory antibodies associated with sterile protection induced by  
controlled human malaria infection. *Cell Microbiol.* **18**, 1739–1750 (2016).
47. Carissimo, G. et al. VCP/p97 Is a proviral host factor for replication of  
chikungunya virus and other alphaviruses. *Front. Microbiol.* **10**, 2236 (2019).

## Acknowledgements

We are indebted to C. Chu, R. McGready and the staff of the Mae Sot Malaria Clinic and the clinics associated with SMRU (Tak Province, Thailand) and the patients attending these clinics. We thank M. Mauduit for help at the beginning of the project. We thank the SigN flow cytometry platform (supported by a grant from the National Research Foundation, Immunomonitoring Service Platform ISP) (NRF2017\_SISFP09). B.R. and B.M. were funded by the Singapore National Medical Research Council (NMRC/CBRG/0047/2013). B.M. was also funded by the Agency for Science, Technology and Research (A\*STAR, Singapore) Young Investigator Grant (BMRC YIG grant no: 13/1/16/YA/009), core funds to SigN from A\*STAR, NUHS Start-up grant (NUHSRO/2018/006/SU/01) and MOE Tier 1 (NUHSRO/2018/094/T1/SEED-NOV/04). L.R. was supported by a Singapore National Medical Research Council IRG grant (NMRC/OFIRG/0065/2018), by a Singapore Immunology Network core research grant and by the Horizontal Programme on Infectious Diseases under A\*STAR. SMRU is supported by The Wellcome Trust of Great Britain as part of the Oxford Tropical Medicine Research Programme of Wellcome Trust–Mahidol University. R.C. acknowledges funding support through the following grants: T1MOE1702 (MOE Tier 1 Grant through the Singapore University of Technology & Design) and RGUOO180301 (Marsden Grant Sub-award through the University of Otago). W.-H.T. was funded by the Australian Research Council Future Fellowship. Duke-NUS Medical School efforts were supported by Singapore's Health and Biomedical Sciences (HBMS) Industry Alignment Fund Pre-Positioning (IAF-PP) grant H18/01/a0/018, administered by A\*STAR.

## Author contributions

B.M. and B.R. carried out the phenotyping characterization of the erythrocytes and the antibody validations for the *P. vivax* invasion assays. G.C., S.W.H., R.S., V.K. and A.S.M.O. developed the *P. vivax* library and performed the erythrocyte binding assays. T.T.T.C., A.S. and R.C. performed and analysed the MS data. J.G. and W.-H.T. carried out construct design and protein purification for the PvRBP2a recombinant proteins and the anti-PvRBP2a monoclonal antibodies. Y.C. and O.B. developed the anti-Duffy antibodies. J.K.Y.C., Y.F. and F.N. were in charge of the management of clinical data. A.E.S., J. Lin, J. Lescar, G.C. and L.F.P.N. managed the biochemistry aspects of the project. S.M.-S. managed the protein modelling of the interaction between CD98 and PvRBP2a. W.N., M.Z.T. and A.-M.C. managed the Octet experiments for CD98 and PvRBP2a interaction measurements. Overall project management was carried out by B.M., B.R. and L.R. The manuscript was prepared by B.M., G.S., B.R. and L.R.

## Competing interests

The authors declare no competing interests.

## Additional information

Extended data is available for this paper at <https://doi.org/10.1038/s41564-021-00939-3>.

Supplementary information The online version contains supplementary material available at <https://doi.org/10.1038/s41564-021-00939-3>.

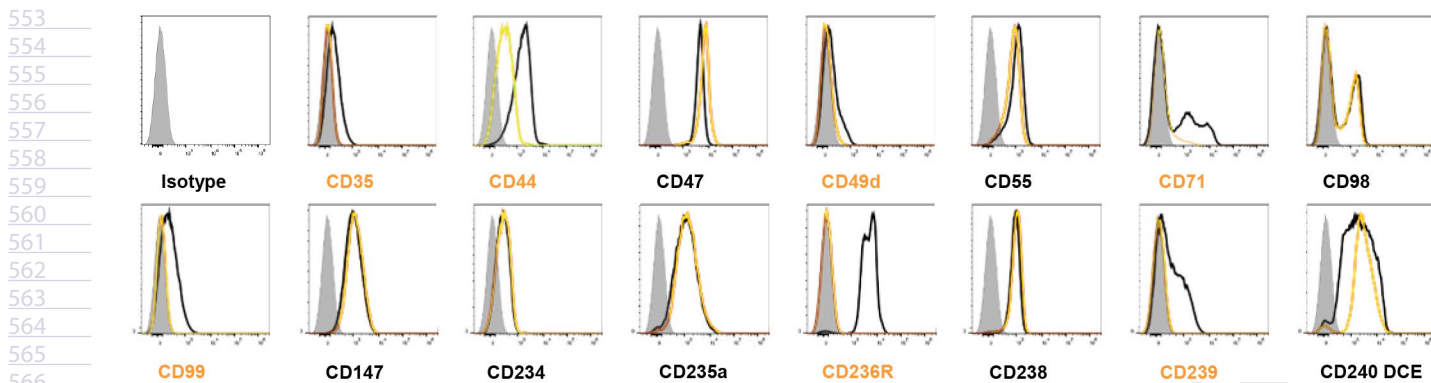
Correspondence and requests for materials should be addressed to B.M. or L.R.

Peer review information *Nature Microbiology* thanks Tuan Tran, Sanjeeva Srivastava and the other, anonymous, reviewers for their contribution to the peer review of this work. Peer reviewer reports are available.

Reprints and permissions information is available at [www.nature.com/reprints](http://www.nature.com/reprints).

Publisher's note Springer Nature remains neutral with regard to jurisdictional claims in published maps and institutional affiliations.

© The Author(s), under exclusive licence to Springer Nature Limited 2021



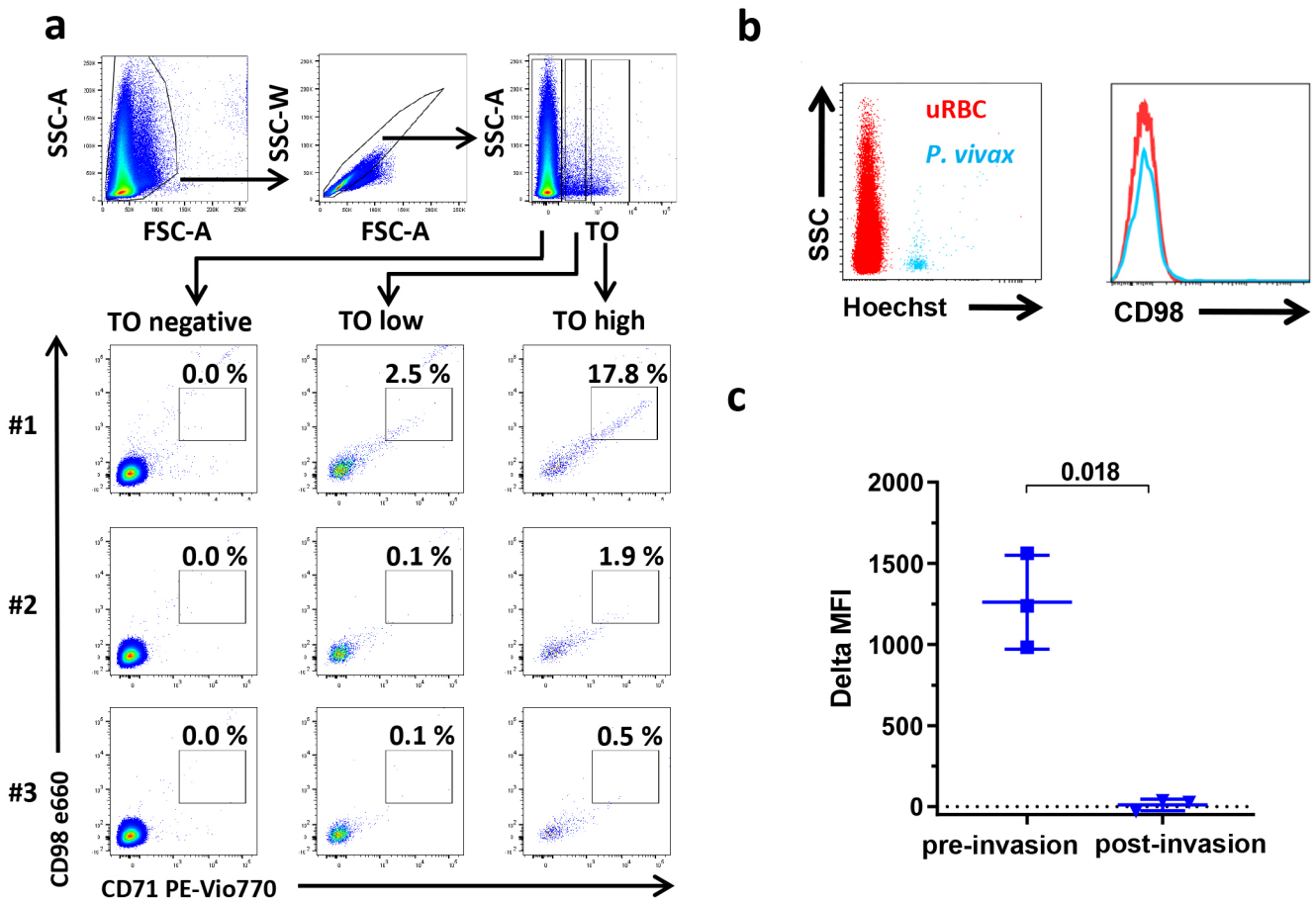
**Extended Data Fig. 1 | Reticulocyte phenotyping.** Trypsin resistance profile of different markers expressed at the surface of cord blood reticulocytes. The black and yellow histograms represent the level of expression before and after trypsin treatment respectively. The trypsin sensitive proteins are annotated in red and the resistant ones in black. The isotype antibody used as control is represented in grey. We used human cord blood samples pre-enriched with reticulocytes and that thus still harbour some normocytes, hence the double peak observed for some proteins such as CD71 and CD98.

553  
554  
555  
556  
557  
558  
559  
560  
561  
562  
563  
564  
565  
566  
567  
568  
569  
570  
571  
572  
573  
574  
575  
576  
577  
578  
579  
580  
581  
582  
583  
584  
585  
586  
587  
588  
589  
590  
591  
592  
593  
594  
595  
596  
597  
598  
599  
600  
601  
602  
603  
604  
605  
606  
607  
608  
609  
610  
611  
612  
613  
614  
615  
616  
617  
618

Uncorrected proof

A

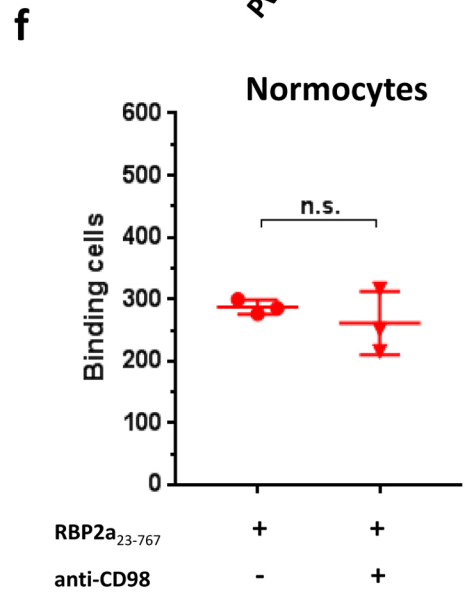
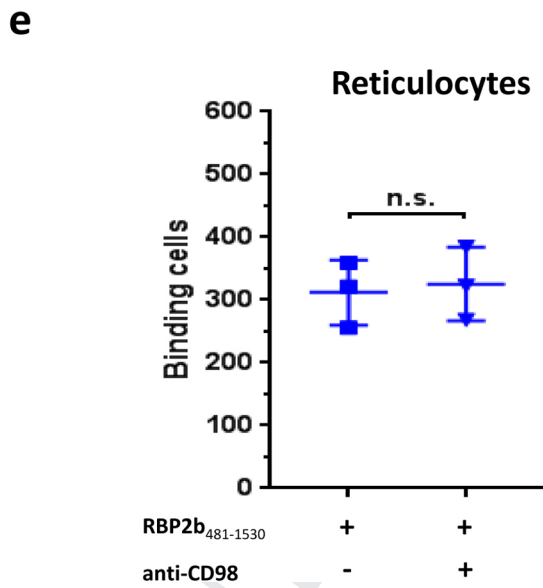
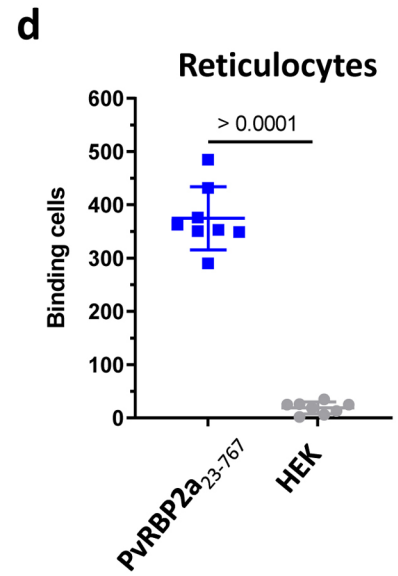
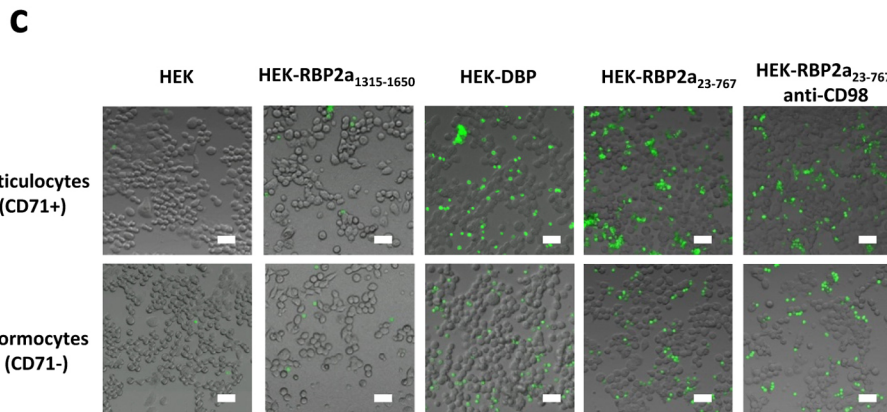
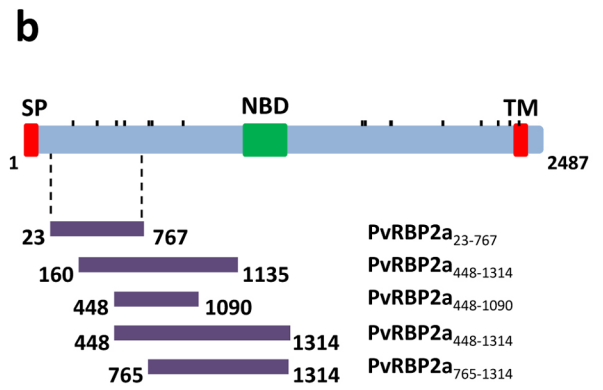
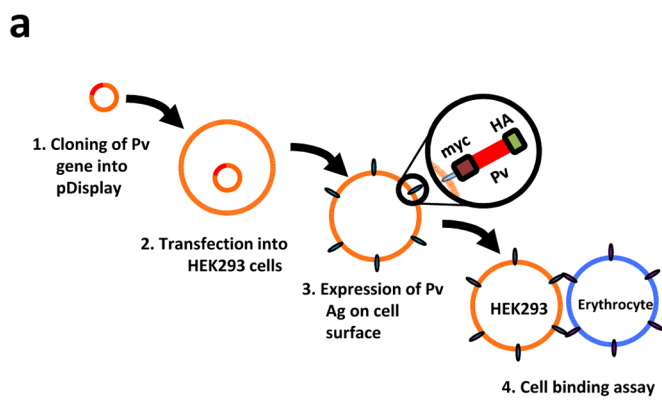
B



**Extended Data Fig. 2 | Flow cytometry analysis of adult peripheral blood, cord blood and *P. vivax* isolates.** **a**, Flow cytometry profile of CD98 and CD71 expression on thiazole orange (TO) negative, low and high erythrocytes for three different human adult peripheral blood samples (forward scatter (FSC) for x-axis and side scatter (SSC) for y-axis). The TO high subset represents the most immature reticulocyte population compared to low subset. **b**, Flow cytometry histogram of CD98 expression (right) at the surface of *P. vivax* rings, early infected reticulocyte forms, gated on Hoechst-positive cells (left), side scatter (SSC) for y-axis. The infected cells positive for Hoechst (a DNA stain) are in blue and the uninfected red blood cells (uRBC), which do not contain DNA, are in red. **c**, Comparison of delta of geometric mean fluorescence intensity (MFI) between immature reticulocytes from three cord blood samples and three vivax infected patients (ring stage), Values are expressed as mean  $\pm$  SD, unpaired Student *t*-test.

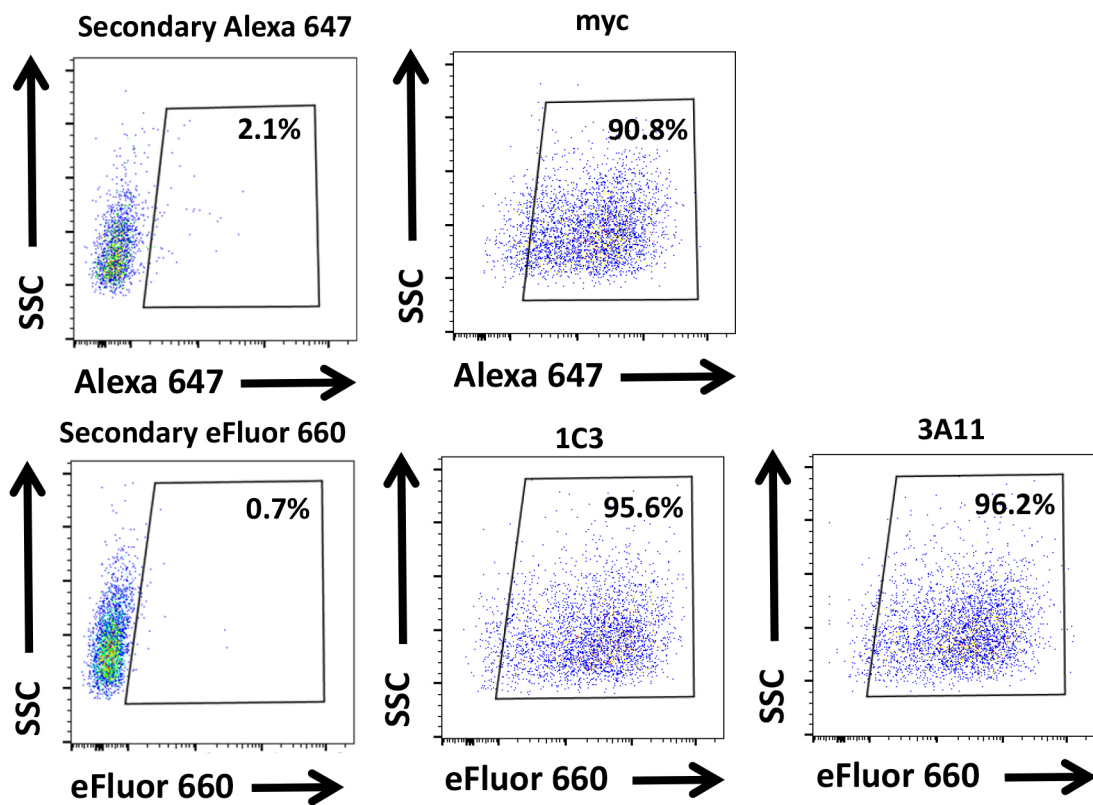


685  
686  
687  
688  
689  
690  
691  
692  
693  
694  
695  
696  
697  
698  
699  
700  
701  
702  
703  
704  
705  
706  
707  
708  
709  
710  
711  
712  
713  
714  
715  
716  
717  
718  
719  
720  
721  
722  
723  
724  
725  
726  
727  
728  
729  
730  
731  
732  
733  
734  
735  
736  
737  
738  
739  
740  
741  
742  
743  
744  
745  
746  
747  
748  
749  
750



Extended Data Fig. 3 | See next page for caption.

751 **Extended Data Fig. 3 | Binding assay of erythrocytes to HEK cells expressing *P. vivax* genes.** **a**, Schematic description of the development of the library  
752 and its use in the erythrocyte binding assay: (1) cloning of *P. vivax* genes in the pDisplay plasmid, (2) transfection of HEK cells, (3) expression of the protein  
753 containing MYC and HA tags at the surface of HEK cells and (5) binding assay with erythrocytes. **b**, Schematic representation of full-length PvRBP2a and  
754 of its recombinant protein fragments used in this study (right). Signal peptide (SP), transmembrane helix (TM) and nucleotide-binding domain (green) are  
755 indicated. The ticks indicated for nonsynonymous SNPs with alternate allele frequency >20%. **c**, Representative images from 3 independent experiments  
756 of binding of reticulocytes (CD71+) or normocytes (CD71-) loaded with the fluorescent dye CFSE to HEK cells expressing the PvRBP2a<sup>1315-1650</sup> (negative  
757 control), Duffy binding protein II (DBPII) fragment or PvRBP2a<sub>23-767</sub> in the presence or absence of anti-CD98 antibodies. The scale represents 50  $\mu\text{m}$ . **d**, The  
758 binding of reticulocytes to HEK transfected with the PvRBP2a<sub>23-767</sub> fragment was done in octuplicate (eight independent experiments) and was shown  
759 to follow a normal distribution as determined by the D'Agostino's K-squared test, and differed significantly from binding to non-transfected HEK cells,  
760 Values are expressed as mean  $\pm$  SD, Student *t*-test. **e**, Binding assays of reticulocytes to HEK cells expressing PvRBP2b<sub>481-1530</sub> in the presence or absence of  
761 anti-CD98 antibodies. (three independent experiments). Values are expressed as mean  $\pm$  SD, no significant differences were observed. **f**, Binding assays  
762 of normocytes to HEK cells expressing PvRBP2a<sub>23-767</sub> in the presence or absence of anti-CD98 antibodies (three independent experiments). Values are  
763 expressed as mean  $\pm$  SD, no significant differences were observed.  
764  
765  
766  
767  
768  
769  
770  
771  
772  
773  
774  
775  
776  
777  
778  
779  
780  
781  
782  
783  
784  
785  
786  
787  
788  
789  
790  
791  
792  
793  
794  
795  
796  
797  
798  
799  
800  
801  
802  
803  
804  
805  
806  
807  
808  
809  
810  
811  
812  
813  
814  
815  
816



**Extended Data Fig. 4 | Antigen specificity of anti-PvRBP2a antibodies.** Mouse 1C3 and 3A11 mAbs recognize specifically the PvRBP2a fragment, PvRBP2a23-767, expressed by HEK cells when tested by flow cytometry. As positive control, rabbit anti-myc antibodies were used. Secondary anti-mouse IgG antibodies coupled with eFluor 660 or mouse anti-rabbit immunoglobulin coupled with Alexa 674 were used as negative control.

# QUERY FORM

<b>Nature Microbiology</b>	
<b>Manuscript ID</b>	[Art. Id: 939]
<b>Author</b>	<b>Benoît Malleret</b>

**AUTHOR:**

The following queries have arisen during the editing of your manuscript. Please answer by making the requisite corrections directly in the e-proofing tool rather than marking them up on the PDF. This will ensure that your corrections are incorporated accurately and that your paper is published as quickly as possible.

<b>Query No.</b>	<b>Nature of Query</b>
Q1:	Please check your article carefully, coordinate with any co-authors and enter all final edits clearly in the eproof, remembering to save frequently. Once corrections are submitted, we cannot routinely make further changes to the article.
Q2:	Note that the eproof should be amended in only one browser window at any one time; otherwise changes will be overwritten.
Q3:	Author surnames have been highlighted. Please check these carefully and adjust if the first name or surname is marked up incorrectly. Note that changes here will affect indexing of your article in public repositories such as PubMed. Also, carefully check the spelling and numbering of all author names and affiliations, and the corresponding email addresses.
Q4:	You cannot alter accepted Supplementary Information files except for critical changes to scientific content. If you do resupply any files, please also provide a brief (but complete) list of changes. If these are not considered scientific changes, any altered Supplementary files will not be used, only the originally accepted version will be published.
Q5:	If applicable, please ensure that any accession codes and datasets whose DOIs or other identifiers are mentioned in the paper are scheduled for public release as soon as possible, we recommend within a few days of submitting your proof, and update the database record with publication details from this article once available.
Q6:	In the sentence "We found that monomeric CD98 interacted with PvRBP2a with a dissociation constant...", please confirm that "dissociation" is meant and not "affinity".
Q7:	For Fig. 4e, please confirm whether the edit of (nm) for Binding to (nM) is ok.
Q8:	Please confirm/correct the styling of the subheading levels in the Methods section
Q9:	In the subsection Criteria for protein identification, please confirm/correct the inserted ref. citation for Chu et al., and check the citation "Supplementary Dataset S2", as is unclear which dataset it is referring to.
Q10:	Please check the sentence 'Hybridomas were cloned by limiting dilution in multwell plates aiming for one cell or fewer per well' for clarity.
Q11:	Please confirm that the edits to the sentence 'Untouched full-size membrane images of the merged channels are provided in the source data' preserve the originally intended meaning.
Q12:	Please confirm/correct the edit of Fig. S2c and Fig. S3d to Extended Data Fig. 2 and Extended Data Fig. 3, respectively, in the Statistical analysis section



# QUERY FORM

<b>Nature Microbiology</b>	
<b>Manuscript ID</b>	[Art. Id: 939]
<b>Author</b>	<b>Benoît Malleret</b>

**AUTHOR:**

The following queries have arisen during the editing of your manuscript. Please answer by making the requisite corrections directly in the e-proofing tool rather than marking them up on the PDF. This will ensure that your corrections are incorporated accurately and that your paper is published as quickly as possible.

<i>Query No.</i>	<i>Nature of Query</i>
Q13:	In the Author contributions section, please check that O.B. is meant to be included here, as there is no name with these initials in the author list.

## Reporting Summary

Nature Research wishes to improve the reproducibility of the work that we publish. This form provides structure for consistency and transparency in reporting. For further information on Nature Research policies, see our [Editorial Policies](#) and the [Editorial Policy Checklist](#).

### Statistics

For all statistical analyses, confirm that the following items are present in the figure legend, table legend, main text, or Methods section.

n/a Confirmed

- |                                     |                                     |  |
|-------------------------------------|-------------------------------------|--|
| <input type="checkbox"/>            | <input checked="" type="checkbox"/> | The exact sample size ( $n$ ) for each experimental group/condition, given as a discrete number and unit of measurement  |
| <input type="checkbox"/>            | <input checked="" type="checkbox"/> | A statement on whether measurements were taken from distinct samples or whether the same sample was measured repeatedly  |
| <input type="checkbox"/>            | <input checked="" type="checkbox"/> | The statistical test(s) used AND whether they are one- or two-sided<br><i>Only common tests should be described solely by name; describe more complex techniques in the Methods section.</i>   |
| <input type="checkbox"/>            | <input checked="" type="checkbox"/> | A description of all covariates tested   |
| <input type="checkbox"/>            | <input checked="" type="checkbox"/> | A description of any assumptions or corrections, such as tests of normality and adjustment for multiple comparisons  |
| <input type="checkbox"/>            | <input checked="" type="checkbox"/> | A full description of the statistical parameters including central tendency (e.g. means) or other basic estimates (e.g. regression coefficient) AND variation (e.g. standard deviation) or associated estimates of uncertainty (e.g. confidence intervals) |
| <input type="checkbox"/>            | <input checked="" type="checkbox"/> | For null hypothesis testing, the test statistic (e.g. $F$ , $t$ , $r$ ) with confidence intervals, effect sizes, degrees of freedom and $P$ value noted<br><i>Give <math>P</math> values as exact values whenever suitable.</i>                            |
| <input checked="" type="checkbox"/> | <input type="checkbox"/>            | For Bayesian analysis, information on the choice of priors and Markov chain Monte Carlo settings   |
| <input checked="" type="checkbox"/> | <input type="checkbox"/>            | For hierarchical and complex designs, identification of the appropriate level for tests and full reporting of outcomes   |
| <input checked="" type="checkbox"/> | <input type="checkbox"/>            | Estimates of effect sizes (e.g. Cohen's $d$ , Pearson's $r$ ), indicating how they were calculated   |

*Our web collection on [statistics for biologists](#) contains articles on many of the points above.*

### Software and code

Policy information about [availability of computer code](#)

**Data collection** The immuno-fluorescent image were processed using LSM software Zen 2009 (Carl Zeiss). Protein probabilities were assigned by the Protein Prophet algorithm described in Analytical Chemistry 2003, 75, 4646-4658. Scaffold (version Scaffold\_4.4.3, Proteome Software Inc., Portland, OR) was used to validate MS/MS based peptide and protein identifications

**Data analysis** The flow cytometry analysis were done on FlowJo software 9.0 (Three Star). The statistical analysis were done on Graph Pad Prism (7.0).

For manuscripts utilizing custom algorithms or software that are central to the research but not yet described in published literature, software must be made available to editors and reviewers. We strongly encourage code deposition in a community repository (e.g. GitHub). See the Nature Research [guidelines for submitting code & software](#) for further information.

### Data

Policy information about [availability of data](#)

All manuscripts must include a [data availability statement](#). This statement should provide the following information, where applicable:

- Accession codes, unique identifiers, or web links for publicly available datasets
- A list of figures that have associated raw data
- A description of any restrictions on data availability

All data are available from the corresponding authors on reasonable request.

## Field-specific reporting

Please select the one below that is the best fit for your research. If you are not sure, read the appropriate sections before making your selection.

Life sciences  Behavioural & social sciences  Ecological, evolutionary & environmental sciences

For a reference copy of the document with all sections, see [nature.com/documents/nr-reporting-summary-flat.pdf](https://www.nature.com/documents/nr-reporting-summary-flat.pdf)

## Life sciences study design

All studies must disclose on these points even when the disclosure is negative.

Sample size	No sample size calculation was performed prior to the study. We used minimum 3 independent experiments to ensure the reproducibility of our results with replicates for each of them. For flow cytometry analysis, a n=3 was used, since each sample collection generated 100.000 single cell data.
Data exclusions	No data were excluded.
Replication	Each experiment was performed minimum three times independently, except for Figure 3a and Figure 2b the experiment was performed twice as mentioned in the legends.
Randomization	As our study is not a clinical trial so we did not perform any randomization. All vivax clinical isolates were collected and used during the duration of the study .
Blinding	No blinding was performed because experimental output with vivax clinical isolates cannot be anticipated.

## Reporting for specific materials, systems and methods

We require information from authors about some types of materials, experimental systems and methods used in many studies. Here, indicate whether each material, system or method listed is relevant to your study. If you are not sure if a list item applies to your research, read the appropriate section before selecting a response.

### Materials & experimental systems

n/a	Involvement in the study
<input type="checkbox"/>	<input checked="" type="checkbox"/> Antibodies
<input type="checkbox"/>	<input checked="" type="checkbox"/> Eukaryotic cell lines
<input checked="" type="checkbox"/>	<input type="checkbox"/> Palaeontology and archaeology
<input type="checkbox"/>	<input checked="" type="checkbox"/> Animals and other organisms
<input type="checkbox"/>	<input checked="" type="checkbox"/> Human research participants
<input checked="" type="checkbox"/>	<input type="checkbox"/> Clinical data
<input checked="" type="checkbox"/>	<input type="checkbox"/> Dual use research of concern

### Methods

n/a	Involvement in the study
<input checked="" type="checkbox"/>	<input type="checkbox"/> ChIP-seq
<input type="checkbox"/>	<input checked="" type="checkbox"/> Flow cytometry
<input checked="" type="checkbox"/>	<input type="checkbox"/> MRI-based neuroimaging

## Antibodies

### Antibodies used

The antibodies commercially available and used for the phenotyping of the erythrocytes are listed in the material and methods (Extended Data Table 5) with details for the clones and the providers.  
 For the P. vivax invasion assay, the camel anti-DARC antibodies were validated and provided by Yves Colin (co-author), Université Sorbonne Paris Cité, Université Paris Diderot, Inserm, INTS, Laboratoire d'Excellence GR-Ex, UMR\_S1134, 6 Rue Alexandre Cabanel, F-75015 Paris, France.  
 For the erythrocyte binding assay and P.vivax invasion the mouse monoclonal antibodies anti-RBP2a were validated and provided by Wai-Hong Tham (co-author), The Walter and Eliza Hall Institute of Medical Research, Parkville, Victoria 3052, Australia.  
 Following antibodies were used for western blots and immunofluorescence imaging rabbit anti-CD98 (Abcam EPR3548, clone EPR3548(2)), rabbit anti-Dematin (Thermo Fisher Scientific PA5-114181, polyclonal) and Alexa Fluor 546-conjugated anti-rabbit secondary antibodies (Invitrogen A-11035).  
 Catalog number for Extended data table 5: CD35 (Becton Dickinson 555451, clone E11), CD44 (Becton Dickinson 555476, clone G44-26 (C26), CD47 (Becton Dickinson 556044, clone B6H12), CD49d (Becton Dickinson 555502, clone 9F10), CD55 (Becton Dickinson 555691, clone IA10), CD71 (Becton Dickinson 555534, clone M-A712), CD71 (Miltenyi 130-115-031, clone REA902), CD98 (Becton Dickinson 556074, clone UM7F8), CD99 (Abcam ab8855, clone 12E7), CD108 (Becton Dickinson 552830, clone KS-2), CD147 (Becton Dickinson 555961, clone HIM6), CD234 (RnD, MAB4139, clone 358307), CD235a (Becton Dickinson 555569, clone GA-R2 (HIR2)), CD236R (Thermo scientific MA5-16592, clone BRIC 4), CD238 (AbD Serotec MCA1987, clone BRIC 203), CD239 (Julien Picot MABS1940-25UG, clone F241) and CD240 DCE (AbD Serotec MCA1981, clone BRIC 69).

### Validation

We added that all antibodies were tested by flow cytometry on human red blood cells excepted rabbit anti-CD98 (Abcam EPR3548, clone EPR3548(2)), rabbit anti-Dematin (Thermo Fisher Scientific PA5-114181, polyclonal). Anti-PvRBP2a were tested on HEK cells by

flow cytometry. Anti-PvRBP2a were tested on HEK cells expressing PvRBP2a by flow cytometry and anti-DARC antibody was validated in Russell et al, Blood 2011 and Malleret et al. Blood 2015 on P. vivax clinical isolates.

## Eukaryotic cell lines

Policy information about [cell lines](#)

Cell line source(s)	ATCC (HEK 293) and Expression Systems (Sf9 insect cell line)
Authentication	The cell lines used were not authenticated.
Mycoplasma contamination	Tested as Mycoplasma free cell line.
Commonly misidentified lines (See <a href="#">ICLAC</a> register)	No commonly misidentified cell lines were used in the study.

## Animals and other organisms

Policy information about [studies involving animals](#); [ARRIVE guidelines](#) recommended for reporting animal research

Laboratory animals	4-6 weeks old female BALB/c and C57BL/6 mice
Wild animals	The study did not involve wild animals.
Field-collected samples	The the study did not involve field samples.
Ethics oversight	Approved by the Walter and Eliza Hall Institute Animal Ethics Committee (2014.009) as described in Gruszczyk et al. Proceedings of the National Academy of Sciences Jan 2016, 113 (2) E191-E200; DOI: 10.1073/pnas.1516512113

Note that full information on the approval of the study protocol must also be provided in the manuscript.

## Human research participants

Policy information about [studies involving human research participants](#)

Population characteristics	The samples were anonymised so we do not have access to clinical and patient data.
Recruitment	Recruitment of vivax infected patients was performed with informed consent at Shoklo Malaria Research Unit in Mae Sot, Thailand. No selection was performed, all consenting patients were recruited. Healthy cord and adult peripheral blood donors were performed with informed consent at KK Women's and Children's Hospital and Singapore Immunology Network respectively. No selection was performed.
Ethics oversight	The ethical guidelines in the approved protocols: OXTREC 45-09 and OXTREC 17-11 from University of Oxford, Centre for Clinical Vaccinology and Tropical Medicine, UK) and MUTM 2008-215 from the Ethics committee of Faculty of Tropical Medicine, Mahidol University. Human cord blood and adult peripheral blood samples were collected under SingHealth CIRB 2019/2443 and 2017/2806 approved protocols respectively and written informed consent was obtained from participants.

Note that full information on the approval of the study protocol must also be provided in the manuscript.

## Flow Cytometry

### Plots

Confirm that:

- The axis labels state the marker and fluorochrome used (e.g. CD4-FITC).
- The axis scales are clearly visible. Include numbers along axes only for bottom left plot of group (a 'group' is an analysis of identical markers).
- All plots are contour plots with outliers or pseudocolor plots.
- A numerical value for number of cells or percentage (with statistics) is provided.

### Methodology

Sample preparation	Red blood cells were stained in PBS with the different antibodies or dyes used for the experiments and the samples were acquired after 20 minutes of incubation without fixation.
Instrument	LSR II flow cytometer (BD Biosciences)
Software	FlowJo software (Three Star)
Cell population abundance	100,000 events per sample



Gating strategy

The gating strategy used for all red blood cell staining is in Figure 1C.

Tick this box to confirm that a figure exemplifying the gating strategy is provided in the Supplementary Information.